Mineralisation of atmospheric CO2 in hydromagnesite in ultramafic mine tailings – Insights from Mg isotopes

Hans C Oskierski, Connor C Turvey, Siobhan A Wilson, Bogdan Z Dlugogorski, Mohammednoor Altarawneh, Vasileios Mavromatis

Mineralisation of atmospheric CO_2 in hydromagnesite in ultramafic mine tailings – insights from Mg isotopes

Hans C. Oskierski[a,b*], Connor C. Turvey[c,d], Siobhan A. Wilson[c,e], Bogdan Z. Dlugogorski[f], Mohammednoor Altarawneh[a], Vasileios Mavromatis[g]

[a]*School of Engineering and Information Technology, Murdoch University, 90 South Street, Murdoch WA, 6150, Australia*

[b]*Geochemistry and Mineral Sciences, Harry Butler Institute, Murdoch University, 90 South Street, Murdoch WA, 6150, Australia*

[c]*School of Earth, Atmosphere and Environment, Monash University, Clayton, Melbourne, VIC 3800, Australia*

[d]*Bradshaw Research Initiative For Minerals & Mining, The University of British Columbia, Vancouver, British Columbia, Canada V6T 1Z4*

[e]*Department of Earth and Atmospheric Sciences, University of Alberta, Edmonton, Alberta, Canada T6G 2E3*

[f]*Office of Deputy Vice-Chancellor, Research & Innovation, Charles Darwin University, Darwin, NT 0909, Australia*

[g]*Géosciences Environnement Toulouse (GET), CNRS, UMR 5563, Observatoire Midi-Pyrénées, 14 Av. E. Belin, 31400 Toulouse, France*

*Corresponding author: H.Oskierski@murdoch.edu.au

Abstract

In this study we present the first Mg isotope data that record the fate of Mg during mineralisation of atmospheric CO_2 in ultramafic mine tailings. At the Woodsreef Asbestos Mine, New South Wales, Australia, weathering of ultramafic mine waste sequesters significant amounts of CO_2 in hydromagnesite [$Mg_5(CO_3)_4(OH)_2 \cdot 4H_2O$]. Mineralisation of CO_2 in above-ground, sub-aerially stored tailings is driven by the infiltration of rainwater dissolving Mg from bedrock minerals present in the tailings. Hydromagnesite, forming on the surface of the tailings, has lower $\delta^{26}Mg$ ($\delta^{26}Mg_{Hmgs}$ = -1.48 ± 0.02 ‰) than the serpentinised harzburgite bedrock ($\delta^{26}Mg_{Serpentinite}$ = -0.10 ± 0.06 ‰), the bulk tailings ($\delta^{26}Mg_{Bulk\ tailings}$ = -0.29 ± 0.03 ‰) and weathered tailings containing authigenic clay minerals ($\delta^{26}Mg_{Weathered\ tailings}$ = +0.28 ± 0.06 ‰). Dripwater ($\delta^{26}Mg_{Dripwater}$ = -1.79 ± 0.02 ‰) and co-existing hydromagnesite ($\delta^{26}Mg_{Hmgs}$ = -2.01 ± 0.09 ‰), forming in a tunnel within the tailings, and nodular bedrock magnesite [$MgCO_3$] ($\delta^{26}Mg_{Mgs}$ = -3.26 ± 0.10 ‰) have lower $\delta^{26}Mg$ than surficial fluid ($\delta^{26}Mg$ = -0.36 ‰) and hydromagnesite.

Complete dissolution of source minerals, or formation of Mg-poor products during weathering, is expected to transfer Mg into solution without significant alteration of the Mg isotopic composition. Aqueous geochemical data and modelling of saturation indices, along with Rayleigh distillation and mixing calculations, indicate that the ^{26}Mg-depletion in the drip water, relative to surficial water, is the result of brucite dissolution and/or precipitation of secondary Mg-bearing silicates and cannot be assigned to bedrock magnesite dissolution. Our results show that the main mineral sources of Mg in the tailings (silicate, oxide/hydroxide and carbonate minerals) are isotopically distinct and that the Mg isotopic composition of fluids and thus of the precipitating hydromagnesite reflects both isotopic composition of source minerals and precipitation of Mg-rich secondary phases. The consistent enrichment and depletion of ^{26}Mg in secondary silicates and carbonates, respectively, underpins the use of the presented hydromagnesite and fluid Mg isotopic compositions as a tracer of Mg sources and pathways during CO_2 mineralisation in ultramafic rocks.

1. Introduction

Ultramafic mine tailings have the ability to capture and bind atmospheric CO_2 in environmentally benign carbonate and hydrotalcite group minerals. Previous studies have demonstrated that CO_2 mineralisation in fine grained Mg-rich waste minerals from asbestos, nickel and kimberlite mines occurs at significantly higher rates compared to natural CO_2 uptake by silicate-weathering (Wilson et al., 2009; Pronost et al., 2011; Oskierski et al., 2013a; Wilson et al., 2014; Mervine et al., 2018; Turvey et al., 2018). This unintentional capture and storage of CO_2 proceeds without additional energy input and is thus considered as a promising option for low-cost, low-energy sequestration of CO_2 to mitigate climate change (e.g., Wilson et al., 2009; Kelemen et al., 2011; Power et al., 2013; Beaudoin et al., 2017; Boschi et al., 2017; Harrison et al., 2019). If tailings facilities are designed to optimise CO_2 uptake, CO_2 sequestration in tailings may be able to render mining operations carbon neutral and provide negative emissions, storing up to 1.5 % of global annual greenhouse gas emissions (Power et al., 2013; Wilson et al., 2014; Siegrist et al., 2017). A detailed understanding of factors limiting natural CO_2 mineralisation, and tools to assess CO_2 storage efficiency, are crucial to unlock the full potential of CO_2 capture and storage in mine tailings. Isotopic compositions have provided key insights into natural carbonation, especially the use of stable carbon isotopes to infer carbon sources and/or kinetic inhibition of CO_2 dissolution into fluids (Wilson et al., 2010; Gras et al., 2017; Turvey et al., 2018) and the use of radiocarbon content to trace atmospheric CO_2 incorporation into mine tailings (Wilson et al., 2009; Oskierski et al., 2013a; Wilson et al., 2014; Oskierski et al., 2016, Turvey et al., 2018).

Magnesium isotopic compositions are significantly fractionated during low temperature processes such as chemical weathering (e.g. Tipper et al., 2006, 2010; Huang et al., 2012), soil forming processes (e.g. Opfergelt et al. 2014), uptake by vegetation (e.g. Opfergelt et al., 2012; Mavromatis et al., 2014a; Pokharel et al., 2017), and carbonate mineral formation (e.g. Immenhauser et al., 2010; Li et al., 2012; Mavromatis et al., 2013), but not during magmatic differentiation and planetary accretion (e.g. Teng et al., 2007; Yang et al., 2009;

Teng et al., 2010). Similarly, the Mg isotopic composition of bulk peridotite, and of primary minerals in peridotite, is not significantly affected by serpentinisation but by weathering and hydrothermal carbonate alteration (Beinlich et al., 2014; Liu et al., 2017; Oelkers et al., 2019; Oskierski et al., 2019). As demonstrated by Oelkers et al., (2019) for injection of CO_2-bearing fluids into basalt, Mg isotopic compositions can thus be used to assess the fate of Mg during weathering and carbonation reactions.

In this study, we present Mg isotopic compositions of mineral and fluid samples that document the mineralisation of atmospheric CO_2 in tailings of the Woodsreef Asbestos Mine, New South Wales, Australia. Our data represent the first record of isotopically distinct mineral sources of Mg in a serpentinised peridotite and they provide a framework for interpreting Mg isotope compositions associated with low temperature alteration of ultramafic rocks, including weathering of bedrock minerals, aqueous speciation of Mg in meteoric fluids and precipitation of hydrated Mg-carbonate minerals. We also report the first Mg isotope data for ultramafic-hosted hydromagnesite and demonstrate that Mg for carbon mineralisation in mine tailings is predominantly derived from the dissolution of silicate and hydroxide minerals rather than from recycling of bedrock carbonates. Our results also show that variations of the Mg isotopic composition of hydromagnesite reflect both the mineral source of Mg in the tailings and the removal of Mg from fluids by precipitation of secondary minerals.

2. Study site and geological background

2.1 New England Orogen

The New England Orogen (NEO) stretches along the central part of the Eastern coast of Australia (Fig. A1). The Southern NEO consists of the Tamworth Belt with Early Devonian to late Carboniferous marine to non-marine, forearc sedimentary and minor volcanic rocks to

the west and the Tablelands Complex with middle Silurian to Carboniferous accretion-subduction metasedimentary and metavolcanic rocks to the east (Vickery et al., 2010; Cawood et al., 2011). These two provinces are separated by the Peel-Manning Fault system (Vickery et al., 2010). The Southern NEO formed by accretion and amalgamation in a convergent plate margin along Eastern Gondwana during late Paleozoic and early Mesozoic times (Cawood et al., 2011).

2.2 Great Serpentinite Belt

The Great Serpentinite Belt (GSB), also called Great Serpentine Belt or Weraerai terrane, is a dismembered ophiolite sequence comprising variably serpentinised harzburgite, dunite and ultramafic melange, together with minor dolerite, plagiogranite, silica-carbonate rock (listvenite), blueschist and eclogite (Aitchison and Ireland, 1995; Ashley, 1997). Crystallisation of parts of the GSB has been constrained to the early Cambrian based on a U-Pb age of zircon in plagiogranite associated to the serpentinite sequence (530 ± 6 Ma; Aitchison and Ireland, 1995) but more recent zircon dating of serpentinite north of Woodsreef suggest formation ages of ~283-277 Ma (Milan et al., 2020). The GSB was emplaced along the Peel-Manning Fault during the early Permian, as indicated by thermal alteration by the Bundarra Plutonic Suite (267.2 ± 1.4 Ma; Cawood et al., 2011) and serpentinite interleaving with the Sakmarian Kensington Formation (Vickery et al., 2010).

2.3 Woodsreef Serpentinite

The Woodsreef Serpentinite, or Woodsreef Melange, crops out as a series of disjointed, fault-bounded blocks with steeply dipping contacts to the Peel-Manning Fault and the Nangarah Formation which dominate the GSB in the study area (Vickery et al., 2010). The Woodsreef Serpentinite hosts the only commercially significant chrysotile mineralisation in

the GSB, which is spatially associated with a North-trending shear zone (Fig. 1; Glen and Butt, 1981; Brown et al. 1992; O'Hanley and Offler, 1992).

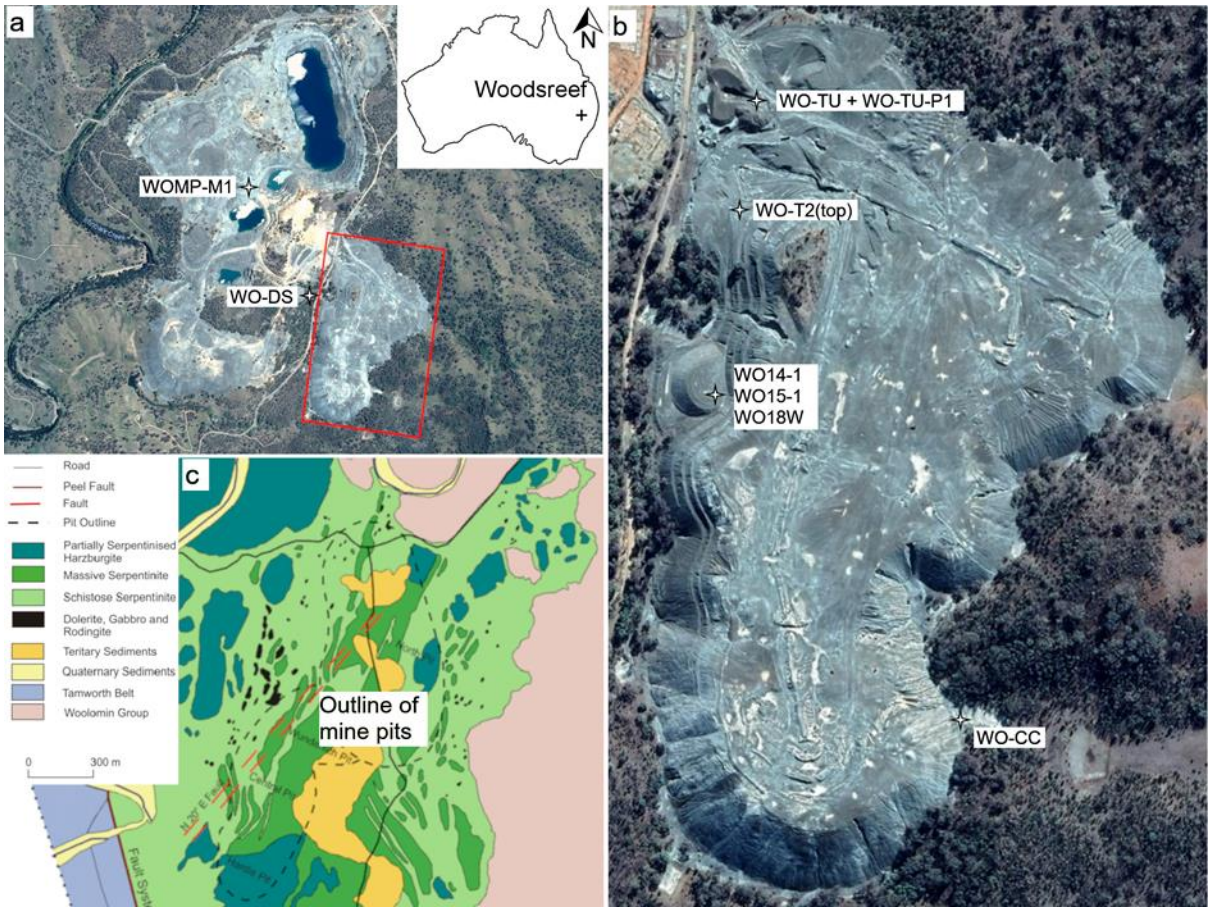

Fig. 1. **a** Aerial view of the Woodsreef Asbestos Mine showing four water-filled mine pits, waste rock dumps in the north-west and south, tailings in the south-east and locations of bedrock magnesite sample WOMP-M1 and water sample WO-DS. The red box shows the location of the tailings (panel b) and the inset shows the location of Woodsreef in northern NSW, Australia. Map data: Google AU. **b** Tailings pile and sampling locations. WO-TU and WO-TU-P1 indicate the location of the tunnel into the tailings. North-south extent of tailings is about 1 km. Map data: Google AU. **c** Geology of the Woodsreef Serpentinite showing lithologic units and outline of mine pits (black dashed line). Figure modified from Davis (2008).

Minor trondhjemite, dolerite, gabbro and rodingite are present in the Woodsreef Serpentinite but partially serpentinised harzburgite, massive serpentinite and schistose serpentinite dominate the bedrock in the mined area (Fig. 1c; Glen and Butt, 1981; Brown et

al. 1992). Minor forsteritic olivine [Mg_2SiO_4], enstatite [$MgSiO_3$] and diopside [$MgCaSi_2O_6$] are remnants of the harzburgite protolith, which has been transformed into serpentinite containing lizardite, chrysotile [$Mg_3Si_2O_5(OH)_4$], magnetite [Fe_3O_4], clinochlore [$(Mg,Fe)_5Al(Si_3Al)O_{10}(OH)_8$] and brucite [$Mg(OH)_2$] during multiple serpentinisation-recrystallisation events (O'Hanley and Offler, 1992). Subsequent hydrothermal alteration of serpentinite to silica-carbonate rock (listvenite) is common in the GSB but not present at Woodsreef (Ashley, 1997; Oskierski et al., 2013a). However, minor nodular, cryptocrystalline magnesite [$MgCO_3$] present in one of the mine pit-walls indicates some carbonation of the bedrock prior to mining (Oskierski et al., 2013a). This nodular, often cauliflower-shaped magnesite (c.f. Fig. 3b in Oskierski et al., 2013c) is commonly associated with magnesite veins, which result from low-temperature (e.g. < 60 ° C) alteration of ultramafic rocks in the GSB (Brown et al., 1992; Ashley, 1997; Oskierski et al., 2013c; 2019).

2.4 CO_2 mineralisation in the Woodsreef mine tailings

Between 1906 and 1983, 550 kt of chrysotile were extracted from the Woodsreef deposit, mostly in large scale open-pit operation (Brown et al., 1992). This resulted in about 24.2 Mt of mine tailings from milling of serpentinite spread out over an area of about 0.5 km^2 (Fig. 1a, b) and a separate 75 Mt of waste rock and weathered overburden (Fig. 1a; Brown et al. 1992; Laughton and Green, 2002). Post-depositional textures observed in the mine tailings can be used to distinguish alteration that occurred after mining from prior alteration of the bedrock (Fig. 2).

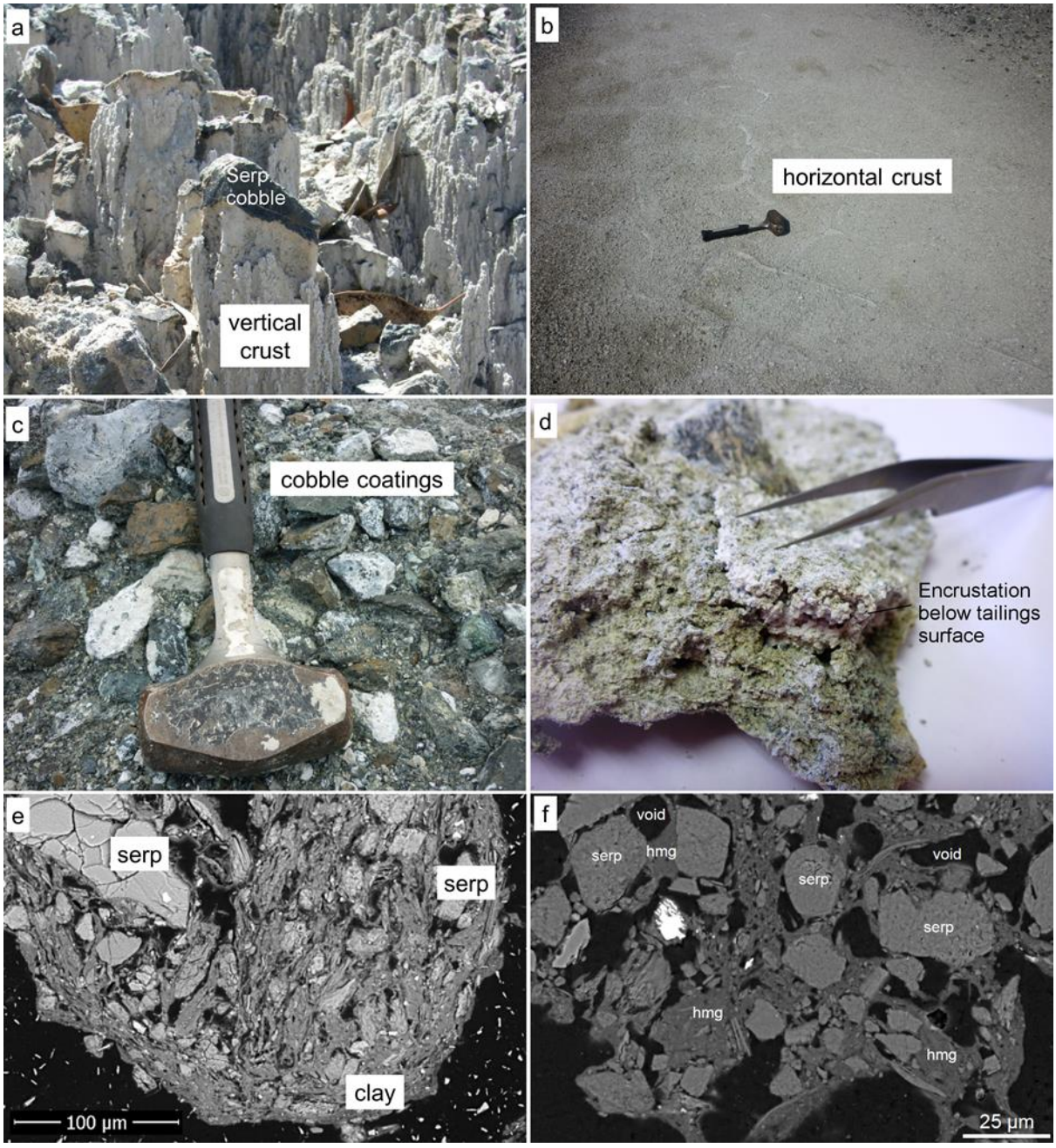

Fig. 2. Post-depositional alteration textures observed in the Woodsreef tailings. **a** Vertical crusts developed on the slope of the tailings. Cobble in the centre is 3-4 cm across. **b** Horizontal crust in depression on top of the tailings. **c** White coatings on serpentinite cobbles at the base of the tailings. **d** Encrustation developed 3-4 cm below tailings surface (Sample WO18). Tweezer tips are about 1 cm apart. **e** Backscatter electron image of cross section through vertical crust showing serpentinite grains cemented by authigenic clay. **f** Backscatter electron image showing serpentinite grains cemented by hydromagnesite (modified from McCutcheon et al., 2017).

These post-depositional textures include vertical crusts (Fig. 2a), resulting from recessive weathering of fine-grained material on the slopes of the tailings, horizontal crusts (Fig. 2b), precipitating due to evaporation of rainwater in depressions on top of the tailings, cobble coatings, forming from moisture-films around serpentinite cobbles (Fig. 2c), and cements binding larger serpentinite fragments both on the surface and within the tailings pile (Fig. 2e, f; Oskierski et al., 2013a; McCutcheon et al., 2017). These textural features are related to the interaction of the fine grained tailings material with CO_2-bearing meteoric waters and hence to weathering after deposition of the tailings. The associated carbon mineralisation represents the most recent fluid-rock interaction in the geological history of the material (Oskierski et al., 2013a). The mineralogy of the tailings changes with depth, with higher contents of carbonates, e.g. hydromagnesite [$Mg_5(CO_3)_4(OH)_2 \cdot 4H_2O$], and lower abundances of brucite at the surface as compared to deeper within the tailings pile (Turvey et al. 2018). This has been interpreted to represent conditions of abundant and limited CO_2 supply during the alteration of brucite, respectively (Oskierski et al., 2016; McCutcheon et al., 2017; Turvey et al., 2018). Hydromagnesite also forms from a drip water that discharges into a tunnel built into the northern part of the tailings (location of sample WO-TU in Fig 1b). The carbonation of ultramafic tailings at Woodsreef can be illustrated through the following set of equations for dissolution of CO_2 (1), dissociation of carbonic acid (2), bicarbonate (3) and water (4), and dissolution or precipitation of serpentine (5), forsterite (6), brucite (7), magnesite (8) and hydromagnesite (9):

$$CO_{2(g)} + H_2O_{(liquid)} \rightleftharpoons H_2CO_{3(aq)} \quad (1)$$

$$H_2CO_{3(aq)} \rightleftharpoons H^+_{(aq)} + HCO_3^-{}_{(aq)} \quad (2)$$

$$HCO_3^-{}_{(aq)} \rightleftharpoons H^+_{(aq)} + CO_3^{2-}{}_{(aq)} \quad (3)$$

$$OH^-_{(aq)} + H^+_{(aq)} \rightleftharpoons H_2O_{(l)} \quad (4)$$

$$Mg_3Si_2O_5(OH)_{4(s)} + 6\,H^+_{(aq)} \rightleftharpoons 3\,Mg^{2+}_{(aq)} + 2\,H_4SiO_{4(aq)} + H_2O_{(l)} \quad (5)$$

$$Mg_2SiO_{4(s)} + 4\,H^+_{(aq)} \rightleftharpoons 2\,Mg^{2+}_{(aq)} + H_4SiO_{4(aq)} \quad (6)$$

$$Mg(OH)_{2(s)} + 2\,H^+_{(aq)} \rightleftharpoons Mg^{2+}_{(aq)} + 2\,H_2O_{(l)} \quad (7)$$

$$MgCO_{3(s)} \rightleftharpoons Mg^{2+}_{(aq)} + CO_3^{2-}{}_{(aq)} \quad (8)$$

$$Mg_5(CO_3)_4(OH)_2{\cdot}4H_2O_{(s)} \rightleftharpoons 5\ Mg^{2+}_{(aq)} + 4\ CO_3^{2-}{}_{(aq)} + 2\ OH^-_{(aq)} + 4\ H_2O_{(l)} \quad (9)$$

The high $\delta^{18}O$, $\delta^{13}C$ and $F^{14}C$ (fraction of modern carbon with $F^{14}C = 1$ equivalent to 100 per cent modern carbon) values of hydromagnesite indicate that it has formed from evaporating rainwaters incorporating atmospheric CO_2, rather than recycled carbon from bedrock carbonates such as magnesite (Oskierski et al., 2013c). A combination of radiocarbon-based tracing of atmospheric CO_2 and quantification of carbonate content based on X-ray diffraction (XRD) data suggests that up to 6900 t of atmospheric CO_2 have been sequestered in the tailings pile since closure of the mine in 1983 (Oskierski et al., 2013a; Turvey et al., 2018).

2.5 Fluids interacting with the mine tailings

Fluids interacting with the tailings can generally be grouped into stream waters, which are associated with ephemeral streams that are intercepted by the tailings, and rainwater, which runs along the surface and percolate through the tailings (Oskierski et al., 2016). Dissolved ions in stream waters may partially originate from the country rock (Ca, Na, K) but Mg concentrations that are about two orders of magnitude higher suggest that Mg in these fluids is predominantly derived from the tailings. This is also consistent with the high reactivity of the tailings that results from the fine grain size (and high surface area) of the material. Rainwaters, responsible for the majority of CO_2 mineralisation, interact only with the tailings (Oskierski et al., 2016). Both types of fluid are moderately alkaline, bicarbonate-dominated and Mg-rich, consistent with typical "Mg-HCO_3" or "Type I waters" that result from the interaction of meteoric water with ultramafic rocks (O'Neil and Barnes, 1971; Bruni et al., 2002; Kelemen et al., 2011; Beinlich and Austrheim, 2012; Oskierski et al., 2016; Paukert Vankeuren et al., 2019). Stable hydrogen and oxygen isotopic compositions relative to local

meteoric water and local evaporation lines demonstrate that only stagnant waters on top and at the base of the tailings have evaporated while the other sampled fluids have not undergone significant evaporation (Oskierski et al., 2016). Due to variable grainsize of the deposited material and varying degrees of cementation and thus pore space and permeability, it is difficult to estimate flow velocities for fluids percolating through the tailings.

Hydromagnesite formed by rainwater has high $\delta^{18}O$ values ($\delta^{18}O_{Hmgs}$ > 26.1 ‰, VSMOW, for vertical and horizontal crusts), suggesting that evaporation is the main process controlling the formation of carbonate crusts on the surface of the tailings (Oskierski et al., 2013c). Inside the tailings, rainwaters partly evolve under CO_2-limited conditions due to the reduced ingress of atmospheric CO_2 into the tailings at depth (Oskierski et al., 2016), as has been observed in other tailings storage facilities (e.g., Gras et al., 2015). Rainwater percolating through the tailings and discharging into a tunnel at the base of the tailings (WO-TU) is thus undersaturated with respect to atmospheric CO_2 (Oskierski et al., 2016). Absorption of atmospheric CO_2 into the drip water together with evaporation control carbonate supersaturation and precipitation in these fluids (Oskierski et al., 2016).

3. Methods

3.1 Samples

Samples were taken from the tailings and the mine pit of the Woodsreef Asbestos Mine. Sampling locations, coordinates, sample type, textural context, mineralogy and the XRD traces of the samples used in this study are shown in Fig. 1 a, b, Table 1 and Fig. A2, respectively.

Table 1
Origin, sample type, textural context and mineralogy of investigated samples

Sample ID	Coordinates Latitude	Longitude	Sample type and textural context	Preparation	Major phases	Minor phases	Trace phases
Bedrock							
WO-CC-S	30.415168	150.741306	Serpentinite cobble, silting pond	picked	Liz[a], Fo		Brc, Mag
WOMP-M1[b]	30.404057	150.733639	Bedrock magnesite, vein in pit	picked	Mgs		Pyr, Liz[a]
Bulk tailings							
WO-T2top	30.409173	150.739281	Bulk tailings	bulk	Liz[a]		Pyr, Mag, Qz, Hmgs
Crusts and coating							
WO14-1-DSC	30.410758	150.739337	Horizontal crust residue	drilled	Liz[a]	Clay	Pyr, Mag, Hmgs
WO14-1CD	30.410758	150.739337	Horizontal carb. crust	picked	Hmgs	Serp	Pyr
WO15-1DSC	30.411086	150.738871	Vertical crust residue	picked	Fo, Serp	Hmgs	
WO15-1-C	30.411086	150.738871	Vertical carb. crust	bulk	Liz[a]	Hmgs	Mag, Pyr, Qz
WO18W	30.410306	150.738501	Carb. encrustation below tailings surface	picked	Hmgs	Liz[a]	Pyr
WO-CC-C	30.415168	150.741306	Carb. crust on cobble, silting pond	picked	Hmgs		Liz[a], Qz, Pyr
WO-TU-P1	30.407788	150.739534	Carb. crust at drip water discharge point	picked	Hmgs	Liz[a]	Pyr
Fluids							
WO-TU	30.407788	150.739534	Drip water discharging into tunnel	unfiltered	*n.a.*	*n.a.*	*n.a.*
WO-DS	30.409505	150.737331	Emerging downstream of tailings	unfiltered	*n.a.*	*n.a.*	*n.a.*

Brc = brucite, Fo = forsterite, Hmgs = hydromagnesite, Liz = lizardite, Mgs = magnesite, Mag = magnetite, Pyr = pyroaurite, Qz = quartz
[a]Small proportions of chrysotile may be present as well, but diagnostic peaks of antigorite are absent (Oskierski et al., 2013c)

[b]Data from Oskierski et al., 2018
n.a. = not applicable

A dark cobble (WO-CC-S) from the base of the tailings and nodular magnesite extracted from the wall of the Central mine pit (WOMP-M1) represent the serpentinised harzburgite bedrock and bedrock carbonate, respectively (Fig. 1a, b; Table 1). Bulk tailings are represented by a sample extracted from a 70 cm deep trench in one of the lower terraces of the tailings pile (WO-T2top; Fig. 1b). Samples of a vertical and a horizontal crust on the tailings, shown in Figs. 2a and b, respectively, were physically split into carbonate-rich fractions (WO14-1-CD, WO15-1-C) and the corresponding carbonate-poor fractions (WO14-1DSC, WO15-1DSC). Sample WO18W is a white, nodular encrustation that has formed 3-4 cm below the surface of the tailings (Fig. 2d). White coatings (WO-CC-C; Fig. 2c) on coarse serpentinite cobbles, form either on the slope of the tailings or within silting ponds at the base of the pile at Woodsreef (Oskierski et al., 2016). A white carbonate crust and drip water have been extracted from a tunnel inside the tailings pile (WO-TUs and WO-TU; Fig. 1b). Water sample WO-DS (Fig. 1b), collected downstream of the tailings, represents a mixture of surface run-off from the tailings but also contributions from ephemeral streams intersected by the tailings. Fluid composition, pH, temperature and aqueous speciation are shown in Table A1. Contributions of Mg to the fluids from external sources are unlikely to be discerned due to the high Mg content and reactivity of the mine tailings (Table A2). Water samples were left to settle for at least 48 h before sub-aliquots for Mg isotope measurements were extracted.

3.2 Sample preparation and characterisation

Some samples were extracted from hand specimens to enrich carbonate-bearing crusts or the associated residual tailings material by picking of grains/fragments while other samples were used in bulk. Both bulk samples and separates were ground in an agate mortar and their mineralogy determined by XRD using a GBC Enhanced Multi-Materials Analyser or a PANalytical Empyrean XRD using Match! Software with the Crystallography

Open or RRUFF databases or PANanalytical HighScore with the ICDD PDF4+ database, respectively.

We further used an acetic acid leach to determine the Mg isotopic composition of the labile carbonate fraction in samples that could not be physically separated. These samples were suspended in excess clean 1 N acetic acid for 1 hour and centrifuged at 3000 rpm for 5 minutes before separation of solid and supernatant by decantation. The supernatant, containing Mg from the labile minerals, was decanted into a Teflon beaker and 0.4 mL of clean concentrated HNO_3 was added and evaporated at low temperature. The leached residue was washed using MilliQ-water and then left to dry. The samples subjected to acetic acid leach consist of hydromagnesite and lizardite, with minor pyroaurite [$Mg_6Fe_2(CO_3)(OH)_{16}{\cdot}4H_2O$], magnetite and quartz (Table 1). Acetic acid is commonly used to selectively dissolve carbonate minerals in the presence of clay minerals (e.g. DePaolo et al., 1983; Poppe et al., 2001) and previous studies have demonstrated that only minor amounts of Mg can be extracted from serpentine minerals in 1 N acetic acid (e.g. Raschman et al., 2007; Teir et al., 2007), while magnetite and quartz can be considered as unreactive.

3.3 Mg isotope analysis

The magnesium isotopic compositions of bulk samples, separates, leachates, leached residues and water were determined following the method described in Mavromatis et al. (2014b). Samples were digested in mixtures of concentrated HNO_3 or HF-HNO_3, evaporated to dryness and dissolved in 1 N HNO_3. About 20 µg of Mg was used for column chemistry in 10 mL Bio-Rad Poly-prep columns for chromatic Mg separation from matrix elements, with > 99 % Mg-recovery achieved. The ratio of cation/Mg of all samples was < 0.001 as determined by ICP-MS. A standard glass cyclonic spray chamber was used for magnesium isotope measurements with a Thermo Scientific 'Neptune' Multi Collector ICP-MS at Géosciences Environnement Toulouse (GET), France. Solutions of ~0.3 M HNO_3 typically

contained Mg concentrations of ~600 ppb, to give intensities of ~10-12 V for ^{24}Mg, while total procedural blanks were generally below 2 mV. Sample-standard bracketing was used for correction of instrumental mass fractionation effects and all data are presented as $\delta^{x}Mg$ with respect to the standard DSM-3 ($\delta^{x}Mg = (^{x}Mg/^{24}Mg)_{sample}/(^{x}Mg/^{24}Mg)_{DSM3}-1) \times 1000$), with x referring to either ^{26}Mg or ^{25}Mg. All of the samples were run in triplicates with the mean values presented in Table 2 along with data for the standards used.

Table 2
Magnesium isotopic composition of analysed samples

Sample ID	Sample type	Mg-fraction	$\delta^{26}Mg_{DSM-3}$ (‰)	2σ	$\delta^{25}Mg_{DSM-3}$ (‰)	2σ	n
Bedrock							
WO-CC-S	Serpentinite cobble	bulk	-0.10	0.06	-0.03	0.03	3
WOMP-M1[a]	Bedrock magnesite	bulk	-3.26	0.10	-1.67	0.01	3
Bulk tailings							
WO-T2top	Bulk tailings	bulk	-0.29	0.03	-0.18	0.03	3
WO-T2top(ac)[b]		acetic	-1.10	0.01	-0.55	0.04	3
WO-T2top(res)[c]		residue	-0.21	0.02	-0.10	0.03	3
Crusts and coatings							
WO14-1-DSC	Horizontal crust non-carb.	bulk	+0.28	0.06	+0.13	0.05	3
WO14-1CD(ac)[b]	Horizontal carb. crust	acetic	-1.47	0.04	-0.75	0.05	3
WO14-1CD(res)[c]		residue	-0.40	0.02	-0.20	0.05	3
WO15-1DSC	Vertical crust non-carb.	bulk	-0.45	0.06	-0.23	0.03	3
WO15-1-C(ac)[b]	Vertical carb. crust	acetic	-1.37	0.03	-0.73	0.03	3
WO15-1-C(res)[c]		residue	-0.27	0.03	-0.14	0.02	3
WO18W(ac)[b]	Carb. encrustation	acetic	-1.58	0.06	-0.83	0.01	3
WO18W(res)[c]		residue	-0.56	0.06	-0.29	0.05	3
WO-CC-C	Carb. crust on cobble	bulk	-1.48	0.02	-0.76	0.03	3
WO-TU-P1	Carb. crust in tunnel	bulk	-2.01	0.09	-1.06	0.05	3
Fluids							
WO-TU	Drip water in tunnel	bulk	-1.79	0.02	-0.95	0.02	3
WO-DS	Stream water	bulk	-0.36	0.04	-0.17	0.02	3
Standards							
JDo-1		bulk	-2.43	0.04	-1.23	0.04	6
BE-N		bulk	-0.27	0.05	-0.14	0.03	3
CAM1		bulk	-2.62	0.06	-1.33	0.05	15
OUMg		bulk	-2.82	0.07	-1.42	0.05	15

[a] Data from Oskierski et al., 2019

[b] Supernatant from acetic acid leach

[c] Residue remaining after acetic acid leach

Replicate δ^{26}Mg analyses of Mg reference standards typically yielded reproducibility better than 0.07 ‰ (2σ). This precision is similar to that reported earlier from our laboratory (e.g. Pearce et al., 2012, Mavromatis et al., 2014a, 2016; Perez-Fernandez et al., 2017; Schott et al., 2016; Beinlich et al., 2018,). Standard materials processed as samples yielded isotopic compositions similar to those reported previously (Table 2), i.e. JDo-1: δ^{26}Mg = -2.35 ± 0.15 ‰, n = 66 (Shalev et al., 2018); BE-N: δ^{26}Mg = -0.41 ± 0.19 ‰, n = 3 (Wombacher et al., 2009); CAM-1: δ^{26}Mg = -2.61 ± 0.05 ‰, n = 247 (Shalev et al., 2018); OUMg: δ^{26}Mg = -2.72 ± 0.02 ‰, n = 3 (Pearce et al., 2012). All error estimates in tables and text are given as 2 standard deviations (2σ).

3.4 Geochemical modelling

PHREEQC (Parkhurst and Appelo, 2013) together with the wateq4f database was used for geochemical modelling of saturation indices and aqueous Mg speciation of waters from the study site (Oskierski et al., 2016). Carbonic acid dissociation constants of Stefansson et al., (2013), the formation constants of $MgCO_3^o$ and $MgHCO_3^+$ determined by Stefansson et al., (2014) and the Mg hydrolysis constant of Palmer and Wesolowski (1997) were included in the database. The distribution of aqueous species was used to estimate the Mg isotopic composition of aqueous Mg^{2+} relative to the bulk fluid, based on the theoretical fractionation factors from Schott et al., (2016) at the measured fluid temperature. Table A1 lists the concentrations of major anions and cations, Mg-speciation, fractions of Mg-species, interpolated fractionation factors for species, as well as the Mg-isotope fractionation and saturation indices calculated for the fluid samples.

4. Results

4.1 Mineralogy

Lizardite and olivine are the dominant minerals in the serpentine cobble WO-CC-S representing the bedrock, with brucite and magnetite present as trace phases (Table 1). This agrees with previous descriptions of the bedrock lithologies and mineralogy at Woodsreef (Glen and Butt, 1981; O'Hanley and Offler, 1992). The nodular bedrock carbonate from the mine pit consists of magnesite, with traces of lizardite and associated pyroaurite (WOMP-M1; Oskierski et al., 2019). Lizardite dominates the bulk tailings sample (WO-T2top) but trace amounts of pyroaurite, magnetite, quartz and hydromagnesite are present.

Horizontal (WO14-1CD) and vertical carbonate-rich crusts (WO15-1-C, WO18W), formed during weathering of the tailings, generally consist of hydromagnesite but contain lizardite as a minor phase along with traces of pyroaurite, magnetite and quartz. The corresponding, physically separated non-carbonate fractions (WO14-1DSC, WO15-1DSC) are dominated by lizardite and olivine, respectively, but WO14-DSC shows a broad low angle feature suggesting the presence of a poorly crystalline clay mineral, whereas WO15-1DSC contains minor hydromagnesite. The cobble coating (WO-CC-C) and crust from the discharge point of drip water into the tunnel (WO-TU-P1) are both composed of hydromagnesite with minor to trace amounts of lizardite, pyroaurite and quartz. Previous studies have consistently identified lizardite (± chrysotile), pyroaurite, hydromagnesite, magnetite, brucite and quartz as the dominant phases present in the tailings at Woodsreef, whereas some common trace phases such as calcite, dolomite, coalingite, chlorite and enstatite are not detected in the current set of samples (Slansky, 1983; Kmetoni, 1984; Oskierski et al., 2013a; 2016; Turvey et al., 2017; 2018).

4.2 Mg isotopic composition of solid samples

The bulk tailings are isotopically lighter (δ^{26}Mg = -0.29 ± 0.03 ‰) than the ultramafic bedrock (δ^{26}Mg = -0.10 ± 0.06 ‰; Table 2). Bedrock magnesite has extremely low δ^{26}Mg, representing the lower end of Mg isotopic compositions recorded for magnesite so far (δ^{26}Mg

= -3.26 ± 0.10 ‰; Oskierski et al., 2019). The physically separated non-carbonate fractions of a horizontal and a vertical crust are isotopically heavier and lighter than the bulk tailings, respectively. The hydromagnesite-crust samples WO-CC-C and WO-TU-P1 both have low δ^{26}Mg (δ^{26}Mg of -1.48 ‰ and -2.01 ‰, respectively) but not as low as the bedrock magnesite.

In all cases the acetic acid leach produces isotopically light leachates, corresponding to the labile fraction of easily decomposed minerals such as hydromagnesite, brucite and pyroaurite, and isotopically heavy residues. For the bulk tailings the labile, acetic leachable fraction is isotopically lighter (δ^{26}Mg = -1.10 ± 0.01 ‰), whereas the acetic-leached residue is only slightly heavier (δ^{26}Mg = -0.21 ± 0.02 ‰) than the bulk composition. The Mg isotopic compositions of leached residues of hydromagnesite-rich crusts (-0.56 ‰ < δ^{26}Mg < -0.21 ‰) are similar to or lighter than the bulk tailings. This indicates that the acetic acid leach may not have completely dissolved all of the labile phases with low δ^{26}Mg and that leached residues may not be used to constrain the Mg isotopic compositions of weathered lizardite or olivine. However, the Mg isotopic composition of labile fractions of hydromagnesite-rich crust samples (-1.58 ‰ < δ^{26}Mg < -1.37 ‰) is consistent with physically separated hydromagnesite samples (-2.01 ‰ < δ^{26}Mg < -1.48 ‰).

4.3 Mg isotopic composition of fluid samples

The results of our previous characterisation of the water samples are summarised in section 2.5 and Table A1. The Mg isotopic composition of stream/run-off water WO-DS (δ^{26}Mg = -0.36 ± 0.04 ‰) is similar, within error, to that of the bulk tailings (δ^{26}Mg = -0.29 ± 0.02 ‰). Drip water sample WO-TU (δ^{26}Mg = -1.79 ± 0.02 ‰) has similarly low δ^{26}Mg as the hydromagnesite samples from the study site, with only a small apparent fractionation of Mg isotopes ($\Delta^{26}Mg_{carbonate\text{-}fluid} = \delta^{26}Mg_{carbonate} - \delta^{26}Mg_{fluid}$ = -0.22 ‰) between the fluid and co-existing hydromagnesite from the drip site (Table 2). Geochemical modelling indicates that

both waters are undersaturated with respect to brucite, hydromagnesite and saturated with respect to magnesite and sepiolite but chrysotile is only supersaturated in WO-TU (Table A1; Oskierski et al., 2016). In WO-TU and WO-DS 70.1 %, 24.4 %, 5.3 % and 91.5 %, 0.9 % and 7.6 % of total Mg occurs as Mg^{2+}, $MgCO_3^o$ and $MgHCO_3^+$ species, respectively (Table A1). Higher fractions of $MgCO_3^o$ and $MgHCO_3^+$ species in WO-TU are a result of the higher pH in WO-TU (pH = 9.1) compared to WO-DS (pH = 7.5).

5. Discussion

5.1 Sources of Mg in the tailings

Mineralisation of CO_2 in post-depositional carbonate crusts and cements in sub-aerially stored tailings is driven by the infiltration of rainwater into the tailings (Wilson et al., 2009; Oskierski et al., 2013a, Wilson et al., 2014; Oskierski et al., 2016; Gras et al., 2017). Both concentration and amount of Mg added to the tailings via rainwater (0.2 mg/L Mg; total of ~ 3 t; Table A2) or as windblown dust (0.22 wt-% MgO; total of ~ 38 to 96 t, Table A2) are negligible compared to the Mg concentration in the fluids resulting from the interaction with the tailings (133 to 158 mg/L Mg; Table A1) and the Mg content in the tailings, respectively (37.3 wt-% MgO; total > 5 Mt, Table A2). This confirms that the Mg for CO_2 mineralisation in hydromagnesite is derived from minerals in the tailings pile.

The mineralogy of freshly deposited, unaltered tailings can be best described as a mixture of remnant phases from the protolith (olivine, pyroxene), phases formed during bedrock serpentinisation (lizardite ± chrysotile, magnetite, brucite) and during low temperature carbonation of the bedrock (magnesite) (Oskierski et al., 2013a; Turvey et al., 2018). In agreement with bedrock lithology (Fig. 1c), samples representing the bulk tailings are dominated by serpentinite, with serpentine (lizardite + chrysotile) making up between 80 and 90 % of bulk tailings samples, magnetite up to 5 % and brucite up to 3 % (Turvey et al.,

2017). Protolith olivine and pyroxene account for up to 5 % and 2.5 %, respectively, while bedrock carbonates occur in trace amounts up to 0.5 % (Oskierski et al., 2013a; Turvey et al., 2017). Accordingly, the δ^{26}Mg of the bulk tailings (δ^{26}Mg = -0.29 ± 0.03 ‰) is only slightly lower than that of the serpentinite bedrock at Woodsreef (δ^{26}Mg = -0.10 ± 0.06 ‰; Table 2; Fig. 3).

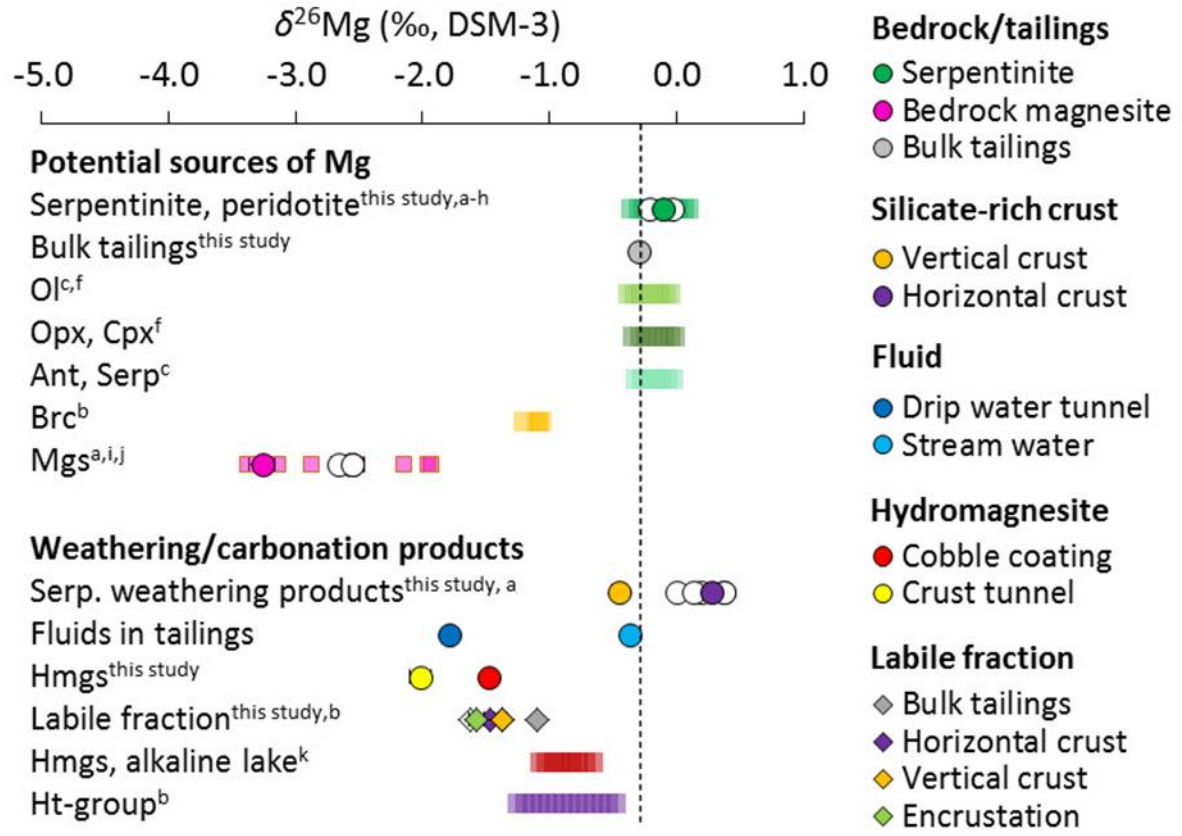

Fig. 3. Magnesium isotopic composition ($\delta^{26}Mg_{DSM}$) of samples from the Woodsreef tailings showing sources of Mg and carbonation products. Samples from Woodsreef and elsewhere in the GSB are shown as full and open symbols, respectively. Boxes and bars correspond to the range of isotopic compositions given in the literature and the dashed line represents the composition of bulk tailings. [a]Oskierski et al., (2019); [b]Turvey, 2018; [c]Beinlich et al., (2014); [d]Hin et al., (2017); [e]Lai et al., (2015); [f]Liu et al., (2017); [g]Pogge von Strandmann et al., (2015); [h]Teng et al., (2010); [i]Ebner et al., (2019); [j]De Obeso et al., (2020); [k]Shirokova et al., (2013). Serp. = serpentinite; Ol = olivine, Opx = orthopyroxene, Cpx = clinopyroxene, Ant = antigorite, Serp = serpentine (unspecified), Brc = brucite, Mgs = magnesite, Hmgs = hydromagnesite, Ht = hydrotalcite.

As illustrated in Fig. 3, Mg isotopic compositions of both bulk tailings and bedrock serpentinite are consistent with pristine terrestrial basalts (e.g. Huang et al., 2015) and

peridotites (e.g. Yang et al., 2009; Beinlich et al., 2014; Pogge von Strandmann et al., 2015), as well as bulk silicate Earth (Fig. 3; Teng et al., 2010; Lai et al., 2015; Hin et al., 2017). Mineral separates of olivine, orthopyroxene, clinopyroxene and antigorite from partly serpentinised ultramafic rocks have similar δ^{26}Mg as bulk peridotites and serpentinites (Fig. 3) and there is no relationship between Mg isotopic composition and degree of serpentinisation (Beinlich et al., 2014; Liu et al., 2017). This suggests that serpentinisation does not significantly affect mineral or bulk rock Mg isotopic composition (Beinlich et al., 2014; Liu et al., 2017), and, consequently, olivine, pyroxene and serpentine in the tailings can be considered to have similar Mg isotopic compositions.

Brucite is a minor (< 3 %, Turvey et al., 2017) but highly reactive component of the mine tailings. Under conditions relevant for rainwater infiltration into the tailings, i.e. ambient temperature and pH 5 to 6, the rates of brucite dissolution (R = 4.68 · 10^{-8} mol m^{-2} s^{-1}, Pokrovsky and Schott, 2004) are about two orders of magnitude higher than those of other potential Mg sources in the tailings, i.e. forsterite (R = 7.08 · 10^{-10} mol m^{-2} s^{-1}, Pokrovsky and Schott, 2000), magnesite (R = 4.49 · 10^{-10} mol m^{-2} s^{-1}, Pokrovsky and Schott, 1999), chrysotile (R = 3.47 · 10^{-12} or 2.09 · 10^{-12} mol m^{-2} s^{-1} based on Mg and Si concentration, respectively, Thom et al., 2013) and magnetite (R = 1.02 · 10^{-10} and 0.31 · 10^{-10} mol m^{-2} s^{-1} for different types of magnetites in White et al. 1994). The inverse relationship of brucite and hydromagnesite abundance with depth in the Woodsreef tailings further points to brucite being a source of Mg for hydromagnesite formation, whereas the homogeneous distribution of magnetite is consistent with its lower reactivity (Turvey et al., 2018). Consequently, brucite is often considered as the primary source of Mg during natural carbonation of mine tailings and it has been linked to increases in pore water pH, carbonation rate and yield, as well as the CO_2 storage capacity of tailings in laboratory carbonation experiments (Pronost et al., 2011; Harrison et al., 2013; Assima et al., 2014; Boschi et al., 2017). At Woodsreef, brucite predominantly occurs in lizardite mesh rims (Offler and O'Hanley, 1992) and could thus not be physically separated for the present study. Micro-analysis of Mg isotopic compositions is

developed for carbonates (e.g. Sadekov et al., 2020) but requires homogeneous and matrix-matched standards which are currently not available for brucite. Natural brucite from the Mount Keith Nickel Deposit in Western Australia has lower $\delta^{26}Mg$ ($\delta^{26}Mg_{brucite}$ = -1.11 ± 0.12 ‰, n = 4; Turvey, 2018) than coexisting serpentine ($\delta^{26}Mg_{serpentine}$ = -0.15 ± 0.42 ‰, n = 3; $\Delta^{26}Mg_{serp\text{-}brucite}$ = -0.96 ‰; Turvey, 2018). Brucite at Mount Keith has formed under similar conditions as at Woodsreef, i.e. serpentinisation of peridotite at temperatures < 350 ° C producing lizardite ± brucite mesh cell textures (Offler and O'Hanley, 1992; Grguric et al., 2001; Barnes et al., 2012), and thus serves as a representative example for the Mg isotopic composition of brucite at Woodsreef.

Traces of magnesite in the tailings and magnesite nodules in the mine pit at Woodsreef indicate limited, low temperature carbonation of the ultramafic bedrock prior to mining (Oskierski et al., 2013b; 2019). The $\delta^{26}Mg$ of nodular magnesite at Woodsreef ($\delta^{26}Mg$ = -3.26 ‰, ± 0.10 ‰), is consistent with that of similar occurrences of low-temperature, ultramafic-hosted magnesite in the GSB ($\delta^{26}Mg$ = -2.73 ‰, ± 0.76 ‰ (2σ), n=4, Oskierski et al., 2019), in Austria ($\delta^{26}Mg$ = -2.36 ‰, ± 0.71 ‰ (2σ), n=7, Kraubath-type magnesite in Ebner et al., 2019), in Oman ($\delta^{26}Mg$ = -3.34 ‰, ± 0.20 ‰ (2σ), n=6, De Obeso et al., 2020) and in Canada ($\delta^{26}Mg$ = -2.50 ‰, ± 0.69 ‰ (2σ), n=4, magnesite rich sediments in Mavromatis et al., 2021). The extreme depletion of ^{26}Mg in this type of magnesite has been ascribed to magnesite dissolution/re-precipitation and the associated Mg isotope fractionation between Mg species in alkaline solutions and to concurrent precipitation of serpentine veins with high $\delta^{26}Mg$ (Oskierski et al., 2019; De Obeso et al., 2020).

Based on the above discussion, we expect three isotopically distinct primary sources of Mg in the tailings:

i) bedrock serpentine (including minor olivine and pyroxene) with $\delta^{26}Mg$ = -0.05 ± 0.20 ‰ (n = 4, this study, Turvey, 2018; Oskierski et al., 2019).

ii) bedrock brucite, which is expected to have lower δ^{26}Mg than bedrock serpentine, with δ^{26}Mg = -1.11 ± 0.12‰ (n=4, for brucite at Mount Keith; Turvey, 2018).

iii) bedrock magnesite with extremely low δ^{26}Mg = -2.72 ‰ ± 0.61 (n=4; Oskierski et al., 2019).

5.2 Mg isotopic constraints on weathering

Weathering transforms serpentinites into clay (Liu et al., 2017; Oskierski et al., 2019). Illite-montmorillionite clays forming during ultramafic rock weathering in the GSB (Oskierski et al., 2019) contain Al-octahedral sheets that are not present in the precursor serpentine. This rearrangement of bonds indicates that the clays have formed by precipitation and not through solid state transformation of serpentine (Eberl, 1984; Beaufort et al., 2015). The formation of Mg-bearing clay minerals controls the Mg isotopic compositions of weathered serpentinites, with preferential retention of ^{26}Mg in the clay structure leading to δ^{26}Mg of up to +0.37 ‰ in the saprolite (Oskierski et al., 2019). Similarly, higher δ^{26}Mg can be observed for the physically separated non-carbonate fraction of a horizontal crust (δ^{26}Mg = +0.28 ‰) on the mine tailings.

Bulk weathered peridotites and serpentinites contain less MgO than their fresh precursors, confirming that Mg is mobile and released into fluids during weathering (Huang et al., 2012; Oskierski et al., 2013b, Liu et al., 2017; Oskierski et al., 2019). Previous studies using Mg isotopes as a tracer of weathering fluxes demonstrate that δ^{26}Mg of riverine Mg is primarily controlled by secondary silicate mineral formation, not by mineral dissolution (e.g. Tipper et al., 2006; Pogge von Strandmann et al., 2008). This is consistent with simple isotope mass balance considerations that dictate that Mg isotopes are not fractionated during complete dissolution of minerals, such as expected for weathering of magnesite or brucite (Mumpton and Thompson, 1966; Moore et al., 2017). Accordingly, measurable changes in fluid Mg isotopic composition require either incorporation of a significant

proportion of Mg into secondary phases or significant Mg isotopic fractionation during secondary phase formation (or a combination thereof).

The formation of relatively Mg-poor montmorillionite-illite clay (molar Mg/Si ratio ~ 0.08, Deer et al., 2013; δ^{26}Mg of 0.35 ‰, Oskierski et al., 2019) during ultramafic rock weathering removes only a small fraction of Mg from the fluid relative to Si. Consequently, the application of Rayleigh-type isotope fractionation models is limited in this context, as about 95 % of Mg remains in the fluid when all the available Si for further clay mineral formation is consumed. Together with the moderate apparent fractionation observed during clay mineral formation from serpentinite ($\Delta^{26}Mg_{clay\text{-}fluid}$ ~ 0.5 ‰, Oskierski et al., 2019), this suggest that ultramafic rock weathering into Mg-poor clay induces only a small reduction in the δ^{26}Mg of the weathering fluid, consistent with the similarity of Mg isotopic compositions of streamwater (δ^{26}Mg = -0.36 ± 0.04 ‰) and bulk tailings (δ^{26}Mg = -0.29 ± 0.03 ‰). However, formation of Mg-rich secondary silicates, such as talc ($[Mg_3Si_4O_{10}(OH)_2]$, molar Mg/Si ratio of 3:4; δ^{26}Mg = +0.17 ‰, Beinlich et al., 2014), "microcrystalline serpentine with stevensite or talc" (waxy vein with molar Mg/Si ratio of 1:1, δ^{26}Mg = +1.19 ‰, De Obeso et al., 2020) or secondary serpentine (molar Mg/Si ratio of 3:2; δ^{26}Mg = +0.96 ‰, De Obeso et al., 2020) can induce significant shifts in the Mg isotopic composition of fluids to lower δ^{26}Mg. Clumped isotope temperatures of carbonates in carbonated and serpentinised peridotite in Oman suggest that some of the above alteration products can form at near-ambient temperatures (De Obeso et al., 2020; Streit et al., 2012).

5.3 Mg isotopic constraints on carbonate formation

The Mg isotopic composition of acetic acid leached, labile fractions of hydromagnesite-rich crust samples and physically separated hydromagnesite samples span a range of δ^{26}Mg from -2.01 ‰ to -1.37 ‰. Secondary carbonates forming during weathering of mine tailings have lower δ^{26}Mg than bedrock serpentine (δ^{26}Mg = -0.10 ± 0.04 ‰), bulk

silicate Earth (δ^{26}Mg = -0.23 ± 0.04 ‰; Lai et al., 2015) and brucite (δ^{26}Mg = -1.11 ± 0.12 ‰) but higher δ^{26}Mg than magnesite (δ^{26}Mg = -3.26 ± 0.10 ‰). Experimental estimates of Mg isotope fractionation between fluids and hydrated Mg-carbonates, including hydromagnesite, dypingite [$Mg_5(CO_3)_4(OH)_2 \cdot 5H_2O$] and nesquehonite [$MgCO_3 \cdot 3H_2O$] are shown in Figure 4 (Mavromatis et al., 2012; Shirokova et al., 2013; Oelkers et al., 2018; Harrison et al., 2021).

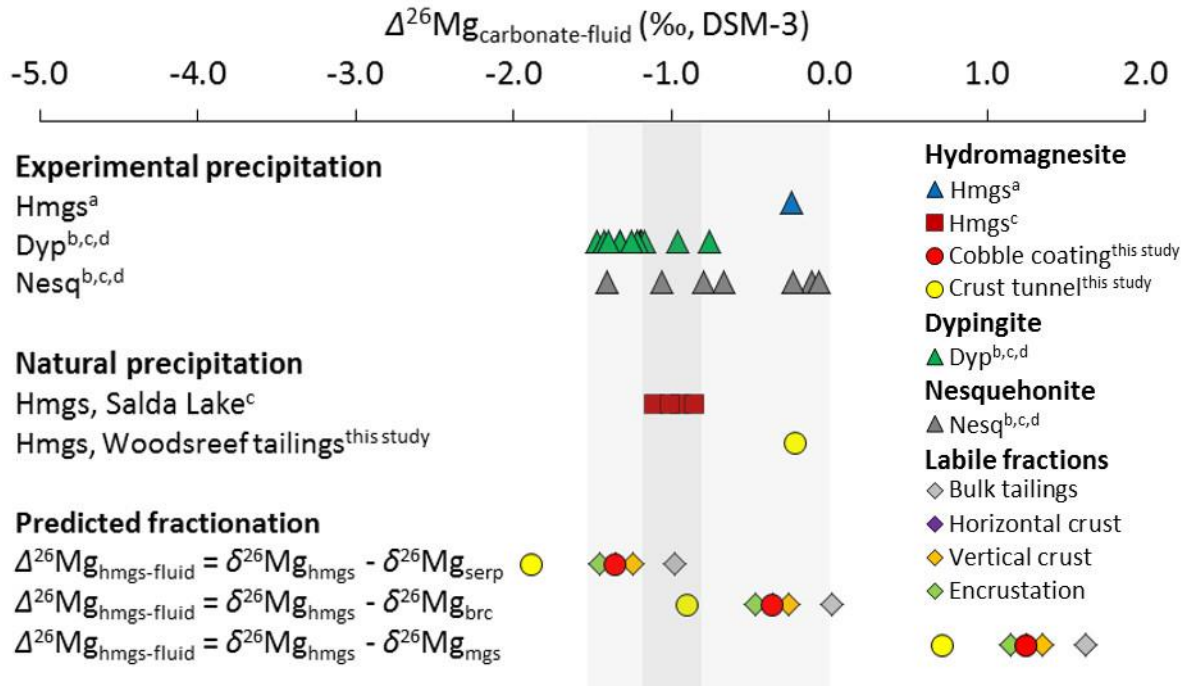

Fig. 4. Effective Mg isotope fractionation between fluid and hydrated Mg-carbonates. Fractionation determined experimentally and based on natural coexisting fluid and Mg-carbonates are shown as triangles and rectangles and as light and dark grey shaded areas, respectively. The apparent fractionation between coexisting dripwater and hydromagnesite forming in the tunnel at Woodsreef is shown separately. Note that δ^{26}Mg values for the horizontal crust (purple diamond) are identical to values for the cobble coating (red circle). Predictions of apparent Mg isotope fractionation ($\Delta^{26}Mg_{hmgs\text{-}fluid} = \delta^{26}Mg_{carbonate} - \delta^{26}Mg_{fluid}$) use the Mg-isotopic compositions of serpentinite (WO-CC-S), brucite (Turvey, 2018) and magnesite (WOMP-M1) to approximate the composition of the fluid, representing scenarios in which the respective mineral dissolves completely and is the only source of Mg for hydromagnesite formation. [a]Oelkers et al., (2018); [b]Mavromatis et al., (2012); [c]Shirokova et al., (2013).

The apparent Mg isotope fractionation between hydromagnesite and co-existing fluid in Salda Lake, Turkey (average $\Delta^{26}Mg_{hmgs\text{-}fluid}$ = -0.99 ± 0.22 ‰ (2σ); range from -1.12 to -0.86 ‰; n = 4), and in the tunnel from Woodsreef ($\Delta^{26}Mg_{hmgs\text{-}fluid}$ = -0.22 ± 0.11 ‰; n = 1) are

within the range of experimentally determined fractionation factors highlighted as light grey shaded area in Figure 4 (Mavromatis et al., 2012; Shirokova et al., 2013; Oelkers et al., 2018; Harrison et al., 2021). Recent work by Schott et al., (2016) suggests that ^{26}Mg preferentially partitions into aqueous Mg-carbonate and Mg-bicarbonate complexes, thus leaving aqueous Mg^{2+} and precipitated Mg-carbonates with lower $\delta^{26}Mg$. Results of geochemical modelling (Table A1) show that the fraction of $MgCO_3^0$ and $MgHCO_3^+$ species in drip water (29.7 % in WO-TU) is higher than in the stream/run-off water (8.5 % % in WO-DS) leading to significantly lower $\delta^{26}Mg$ of Mg^{2+} in drip water ($\delta^{26}Mg_{Mg2+}$ = -3.33 ‰) than in stream/run-off water ($\delta^{26}Mg_{Mg2+}$ = -0.74 ‰), respectively. Consequently, hydromagnesite precipitated from the drip water would be expected to have lower $\delta^{26}Mg$ than that precipitated from stream/run-off water, consistent with our data for hydromagnesite formed in the tunnel ($\delta^{26}Mg$ = -2.01 ± 0.09 ‰; n = 1) and on the surface of the tailings ($\delta^{26}Mg$ = -1.48 ± 0.02 ‰; n = 1).

Besides inter-species fractionation, kinetic effects may be responsible for the wide range of observed fractionation factors between hydrated Mg-carbonates and fluid ($\Delta^{26}Mg_{carbonate\text{-}fluid}$ between -1.43 ‰ to -0.07 ‰, Fig. 4; Mavromatis et al., 2012; Shirokova et al., 2013; Oelkers et al., 2018; Harrison et al., 2021). Experimental studies show that kinetic effects tend to reduce Mg isotope fractionation between fluid and precipitated carbonates compared to equilibrium conditions (Immenhauser et al., 2010; Mavromatis et al., 2013; Pearce et al., 2012). Similarly, the small apparent isotope fractionation between coexisting drip water and hydromagnesite from the tunnel at Woodsreef ($\Delta^{26}Mg_{hmgs\text{-}fluid}$ = -0.25 ‰) may reflect kinetic effects obscuring equilibrium isotope fractionation, as well as the associated inter-species fractionation, during fast precipitation.

Laboratory precipitation experiments have shown that the Mg isotope compositions of hydrated Mg carbonates can be reset on short time scales (Harrison et al., 2021), which suggests that hydromagnesite in the mine tailings reflects the most recent fluid Mg isotopic composition. However, it is unlikely that the fluid Mg isotopic composition has changed

significantly over the 30 years since tailings deposition, unless a highly reactive phase, such as brucite, would have been dissolved completely. Mineralogical depth profiles indicate some depletion of brucite towards the surface, potentially affecting surface waters and hydromagnesite, but also demonstrate that brucite is still present in the analysed profiles after 30 years of weathering (Turvey et al., 2018). Furthermore, fluid volumes passing through the tailings in the semi-arid climate at Woodsreef are low and, consequently, the tailings are rock-buffered, as opposed to fluid-buffered conditions in laboratory experiments (Harrison et al., 2021). Mg exchange between fluid and solid, and thus the resetting of isotope compositions of hydrate Mg-carbonates, has been shown to be limited in similar mineral-buffered systems (Mavromatis et al., 2021).

Anhydrous carbonates (calcite, dolomite and magnesite) have lower $\delta^{26}Mg$ than the fluids they precipitated from, both in natural and laboratory settings (e.g. Immenhauser et al., 2010; Li et al., 2012; Pearce et al., 2012; Mavromatis et al., 2013; 2014b; Schott et al., 2016; Mavromatis et al., 2017; Pogge von Strandmann et al., 2019). Similarly, all experimental and natural records of Mg isotope fractionation between fluid and hydrated Mg-carbonate ($\Delta^{26}Mg_{carbonate\text{-}fluid} = \delta^{26}Mg_{carbonate} - \delta^{26}Mg_{fluid}$) show lower $\delta^{26}Mg$ in the precipitated carbonate than in the fluid (Fig. 4; this study, Shirokova et al., 2011; Mavromatis et al., 2012; Shirokova et al., 2013; Oelkers et al., 2018; Harrison et al., 2021), suggesting that hydromagnesite at Woodsreef has lower $\delta^{26}Mg$ than the fluid from which it has precipitated.

As a first approximation, apparent fractionation between hydromagnesite and fluid ($\Delta^{26}Mg_{hmgs\text{-}fluid}$) is calculated by approximating $\delta^{26}Mg_{fluid}$ as $\delta^{26}Mg_{serp}$, $\delta^{26}Mg_{brc}$ or $\delta^{26}Mg_{mgs}$, respectively, to represent the different mineral sources of Mg in the tailings. This approximation assumes that these minerals dissolve completely during weathering, provide the main source of Mg to the fluid without mixing and that hydromagnesite is the only secondary phase precipitated. Apparent fractionation between hydromagnesite and fluid is broadly consistent with experimental fractionation factors (average $\Delta^{26}Mg_{carbonate\text{-}fluid}$ = -1.00 ± 0.85 ‰ (2σ); range from -1.43 to -0.07 ‰; n = 26; Mavromatis et al., 2012; Shirokova et al.,

2013; Oelkers et al., 2018; Harrison et al., 2021) if serpentine (average $\Delta^{26}Mg_{hmgs\text{-}serp}$ = -1.38 ± 0.60 ‰; range from -1.9 to -1.0 ‰) or brucite (average $\Delta^{26}Mg_{hmgs\text{-}brc}$ = -0.39 ± 0.60 ‰; range from -0.9 to -0.0 ‰) are the main sources of Mg to the fluid (Fig. 4). Apparent fractionation is clearly inconsistent with experimental constraints if magnesite is the source of Mg to the fluid (average $\Delta^{26}Mg_{hmgs\text{-}mgs}$ = +1.22 ± 0.60 ‰; range from +0.7 to +1.6 ‰; Fig. 4). Importantly, incorporation of Mg from magnesite dissolution into hydromagnesite would require strong enrichment of ^{26}Mg either in the fluid (see next section) or during precipitation, opposing previously determined fractionation factors between hydrated Mg-carbonates and fluid (Mavromatis et al., 2012; Shirokova et al., 2013; Oelkers et al., 2018; Harrison et al., 2021).

5.4 Chemical and isotopic constraints on fluid evolution in ultramafic mine tailings

Mg isotopic compositions of fluids interacting with the mine tailings reflect dissolution and mixing of Mg from mineral sources in the tailings as well as subsequent precipitation of secondary minerals. Context for interpretation of Mg isotopes is provided by the chemical, H, C and O isotopic compositions of fluids from the mine tailings presented in previous work (Oskierski et al., 2016).

Water sample WO-DS represents contributions from both surface run-off and ephemeral streams intersected by the tailings (Oskierski et al., 2016). The explanation for high DIC concentration and low $\delta^{13}C$ DIC in this fluid (Table A3) is equivocal as it could result either from magnesite dissolution, or, alternatively, from dissolution of soil CO_2. The Mg isotopic composition ($\delta^{26}Mg_{fluid}$ = -0.36 ± 0.04 ‰) of the fluid is similar to that of the bulk tailings ($\delta^{26}Mg_{bulk\ tailings}$ = -0.29 ± 0.03 ‰). Accordingly, Mg-isotope based mixing calculations, such as

$$\delta^{26}Mg_{fluid} = f\,\delta^{26}Mg_{source1} + (1\text{-}f)\,\delta^{26}Mg_{source2}$$

with *f* referring to the mole fraction of Mg from source 1, indicate high contributions of Mg from serpentine dissolution (92 to 72 %; $\delta^{26}Mg_{Serpentine}$ = -0.10 ± 0.06 ‰) and low contributions from either magnesite (8 %; $\delta^{26}Mg_{Mgs}$ = -3.26 ± 0.10 ‰), hydromagnesite (19 %; $\delta^{26}Mg_{Hmgs}$ = -1.48 ± 0.02 ‰) or brucite (26 %; $\delta^{26}Mg_{Brc}$ = -1.11 ± 0.12 ‰), respectively (Table A4). This is generally consistent with the presence of Mg, Si and DIC in the fluid and with increasing saturation indices of the fluid with respect to chrysotile, magnesite, hydromagnesite and brucite (Table A1) relative to unreacted rainwater (sample MWT in Oskierski et al., 2016).

The influence of secondary mineral precipitation on the Mg isotopic composition of the fluid can be assessed through Rayleigh fractionation (Fig. 5) based on a set of assumptions, such as constant fractionation factors for mineral precipitation along the fluid pathway and the maintenance of supersaturation with respect to the mineral due to evaporation and ingress of CO_2 from the atmosphere. The Rayleigh model is further based on the Mg isotopic composition of the bulk fluid and does not consider changes in Mg speciation due to precipitation and the associated changes in the isotopic composition of Mg^{2+} ions (Schott et al., 2016).

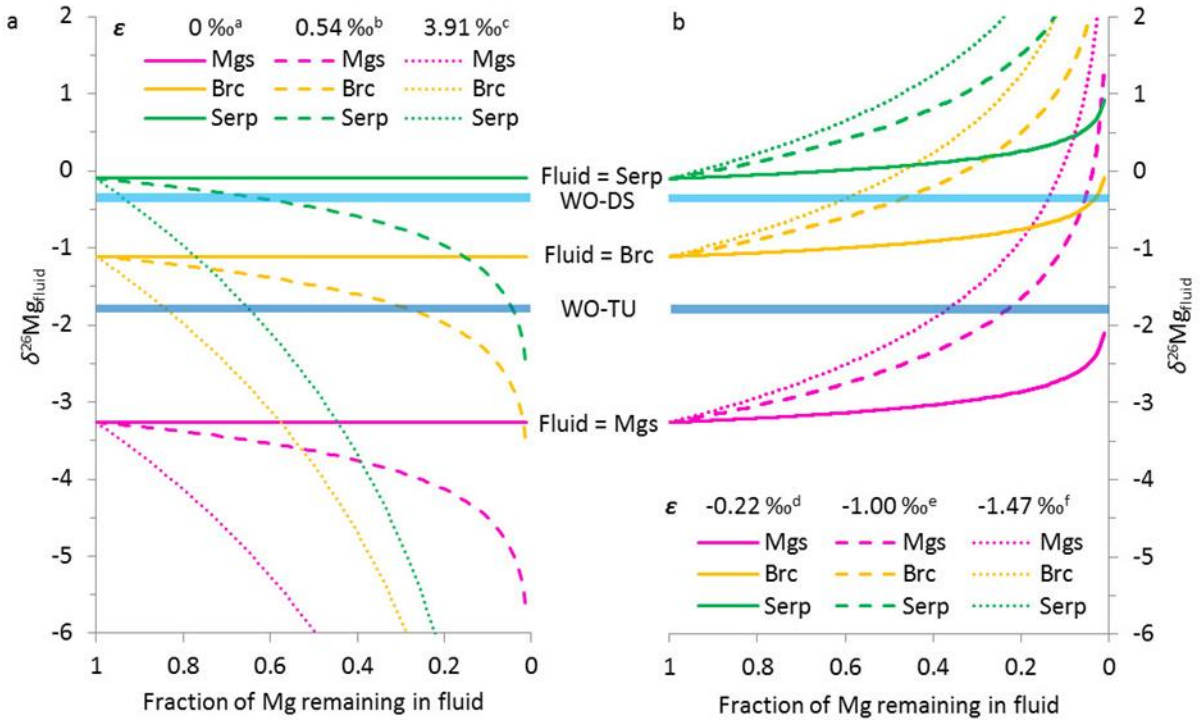

Fig. 5 Rayleigh model for the development of the Mg isotope composition of fluids **a** during precipitation of secondary silicates with high δ^{26}Mg and **b** during precipitation of hydromagnesite with low δ^{26}Mg. The δ^{26}Mg of the fluid is calculated using $\delta_{reactant} = \delta_0 + \varepsilon \ln f_r$, where δ_0 is the initial fluid composition based on dissolution of serpentine, brucite or magnesite, respectively, ε is the isotopic enrichment factor and f_r the fraction of Mg remaining in the fluid. Isotopic enrichments ε are based on [a]Beinlich et al., (2014), no enrichment between forsterite and serpentine; [b]Oskierski et al., (2019) and Ryu et al., 2016, enrichment of ^{26}Mg in clay minerals; [c]Wang et al., (2019), calculated enrichment during lizardite precipitation; [d]this study, coexisting fluid and hydromagnesite in tunnel; Oelkers et al., 2018, hydromagnesite precipitation experiment; [e]Shirokova et al., (2013), coexisting fluid and hydromagnesite in Lake Salda; [f]Mavromatis et al., (2012), strongest enrichment during abiotic precipitation of dypingite; Mgs = magnesite; Brc = brucite; Serp = serpentine.

Consistent with mixing calculations (Table A3), derivation of the fluid Mg from magnesite and subsequent Rayleigh fractionation into the observed composition would require 86 % and 94 % of Mg to precipitate to achieve the observed fluid isotopic composition ($\delta^{26}Mg_{Fluid}$ = -0.36 ± 0.04 ‰), considering the maximum experimental ($\Delta^{26}Mg_{carbonate\text{-}fluid}$ = -1.43 ‰; Mavromatis et al., 2012) and the natural ($\Delta^{26}Mg_{carbonate\text{-}fluid}$ = -1.0 ‰; Shirokova et al., 2013) estimates of fractionation between hydrated carbonate and fluid,

respectively (intersection of dotted and dashed lines with WO-DS in Figure 5b). This requires the initial fluid to have Mg concentrations in the g/L range, which is at least an order of magnitude higher than previously observed in fluids associated with ultramafic rocks (e.g. < 88.5 mg/L, Beinlich and Austrheim, 2012; <15.4 mg/L Mg, Cipolli et al., 2004; 57.1 mg/L Mg, Paukert Vankeuren et al., 2019) or carbonate dissolution in karst environments (e.g. < 223.1 mg/L Ca, Samanta et al., 2015; < 250 mg/L Ca, Zhao et al., 2015). Furthermore, it is impossible for a magnesite-derived fluid to attain the observed fluid Mg isotopic composition if the apparent (and potentially kinetically controlled) fractionation observed in this study ($\Delta^{26}Mg_{carbonate\text{-}fluid}$ = -0.22 ‰) is used in Rayleigh fractionation calculations (solid pink line in Figure 5b). Lower initial fluid δ^{26}Mg, resulting from a higher contribution to fluid Mg from brucite dissolution, could be realistically compensated by Rayleigh distillation during hydromagnesite precipitation to achieve the observed fluid Mg isotope composition (yellow lines in Figure 5b). Overall, the low Mg/DIC and high Mg/Si ratios of WO-DS are similar to Mg-HCO_3 (type I) waters, which dissolve carbonate-free, brucite-bearing serpentinite in an open system with respect to atmospheric CO_2 (e.g. Bruni et al., 2002; Cipolli et al., 2004). Magnesium isotopic compositions thus show that the additional DIC in the fluid is predominantly derived from soil CO_2 rather than bedrock magnesite dissolution (Oskierski et al., 2016).

As for WO-DS on the surface of the tailings, interaction of rainwater with the tailings increases the saturation state of the drip water (WO-TU) with respect to chrysotile, brucite, hydromagnesite and magnesite (Table A1), confirming that dissolution of these minerals may contribute Mg to the fluid. Mixing calculations using serpentine (δ^{26}Mg = -0.10 ± 0.06 ‰) as the high δ^{26}Mg endmember suggest that up to 54 % and 89 % of the Mg in the drip water (δ^{26}Mg = -1.79 ± 0.02 ‰) could be derived from the dissolution of magnesite (δ^{26}Mg = -3.26 ± 0.10 ‰) and hydromagnesite (δ^{26}Mg = -2.01 ± 0.9 ‰), respectively (Table A4). If brucite (δ^{26}Mg = -1.11 ± 0.12 ‰) is considered as the high δ^{26}Mg endmember, magnesite and

hydromagnesite dissolution could contribute up to 32 % and 66 % of Mg, respectively (Table A4).

However, simple mixing of Mg from different mineral sources is inconsistent with the low DIC, the observed undersaturation of the fluid relative to atmospheric CO_2 and the high $\delta^{13}C$ and ^{14}C content of the fluid (Oskierski et al., 2016). Fluids draining carbonate-bearing terrain are commonly strongly saturated with CO_2 and thus prone to degas (e.g. Jin et al., 2015; van Geldern et al. 2015; Zhao et al., 2015), whereas the drip water in the tailings absorbs CO_2 from the atmosphere (Oskierski et al., 2016). Similarly, dissolution of magnesite and subsequent increase in fluid $\delta^{26}Mg$ through Rayleigh type fractionation during hydromagnesite precipitation (pink lines in Figure 5b) would require CO_2 saturation within the tailings and in the fluid and would result in carbon isotopic compositions influenced by bedrock carbonate. On the other hand, high $\delta^{13}C$ and ^{14}C content demonstrate that drip water DIC is derived from atmospheric CO_2, not bedrock carbonate dissolution, with carbon isotope mixing calculations suggesting atmospheric contributions of 80 % and 100 %, respectively (Table A3, A4). Supersaturation with respect to magnesite and focussed precipitation of hydromagnesite at the discharge point of the fluid into the tunnel thus result from an increase in pH due to tailings mineral dissolution under CO_2-limited conditions and subsequent uptake of atmospheric CO_2 into the fluid (Oskierski et al., 2016). The increase in pH, high Mg/Si ratios, high $\delta^{13}C$, high ^{14}C and undersaturation with respect to atmospheric CO_2 can be best explained by the dissolution of highly reactive brucite (Oskierski et al., 2016), which also provides a low $\delta^{26}Mg$ source of Mg (Fig. 3). Consequently, Mg from magnesite can only be a minor source for CO_2 mineralisation in hydromagnesite.

Depth profiles in the tailings pile indicate that hydrotalcite-group minerals may form through fluid-mediated carbonation of brucite under CO_2 limited conditions (Turvey et al., 2018). The Mg isotope fractionation associated with transformation of brucite to hydrotalcite is not well understood yet, but the presence of hydrotalcite minerals with higher $\delta^{26}Mg$ than brucite (Fig. 3; Turvey, 2018), suggests that hydrotalcite may preferentially incorporate ^{26}Mg,

thereby decreasing δ^{26}Mg in the fluid. Considering the strong supersaturation of the drip water with respect to chrysotile (and sepiolite, Table A1), the high fluid Mg/Si ratio relative to serpentine stoichiometry and the presence of authigenic Mg clay in the tailings (Fig. 2e), the depletion of ^{26}Mg in the fluid WO-TU is also consistent with precipitation of secondary silicate phases with high molar Mg/Si ratio and high δ^{26}Mg along the fluid flow path. The observed fluid chemical and isotopic composition can thus be best reconciled with brucite and serpentine dissolution in a closed system with respect to atmospheric CO_2 along with Rayleigh fractionation preferentially removing ^{26}Mg (and Si) into secondary silicate phases (dotted and dashed green and yellow lines in Fig. 5a; Oelkers et al., 2019; Oskierski et al., 2019).

6. Implications and concluding remarks

Our record of Mg isotopic compositions from the Woodsreef Asbestos Mine provides insight into the mineralisation of atmospheric CO_2 in carbonate crusts and coatings on ultramafic mine tailings. Air capture and mineralisation of CO_2 in ultramafic mine tailings can substantially contribute to off-setting emissions of mining operations and combatting increasing atmospheric CO_2 concentrations (e.g. Wilson et al., 2009; Oskierski et al. 2013; Power et al., 2013; Wilson et al., 2014; Gras et al., 2015; Turvey et al., 2018). However, a large proportion of the CO_2 storage potential of ultramafic mine tailings currently remains untapped, as natural weathering reactions predominantly dissolve Mg from brucite, which is highly reactive but much less abundant than Mg-bearing silicate minerals (e.g. Harrison et al., 2013; Wilson et al., 2014; Turvey et al., 2018). In addition, the dissolution of Mg from pre-existing carbonate minerals may reduce the net amount of CO_2 stored in the mine tailings (Wilson et al., 2009; Oskierki et al. 2013a). The ability to trace Mg during CO_2 mineralisation is thus critical for the monitoring of the interaction between fluids and tailings minerals and

for the development of more effective mineral carbonation processes, as demonstrated by Oelkers et al., (2019).

The data described here represent a framework for interpreting Mg isotopic compositions with respect to Mg sources and fluid evolution during ultramafic rock carbonation. We observe that the Mg isotopic compositions of the mineral groups relevant for carbonation of ultramafic rocks and tailings, such as silicates (serpentine, olivine, pyroxene), oxides/hydroxides (brucite) and carbonates (magnesite, calcite, dolomite), are distinct. Despite the large variation in natural carbonates (and potentially in natural brucite) that may result from Rayleigh type distillation effects on fluid compositions, Mg isotopic compositions of carbonates and brucite are clearly different from those of Mg silicates, providing the ability to distinguish the most relevant sources of Mg for CO_2 mineralisation in ultramafic rocks. Carbon concentrations and isotopic compositions, particularly radiocarbon, remain critical for explaining the fate of carbon during ultramafic rock carbonation in ultramafic mine tailings (Wilson et al., 2009; Oskierski et al., 2013c) but, compared to Mg isotopic compositions, provide limited insights into the interaction of fluids with Mg silicate minerals.

The use of Mg isotopes to trace Mg during silicate carbonation is underpinned by the consistent enrichment and depletion of ^{26}Mg during formation of secondary silicate and carbonate minerals, respectively, documented for both low temperature (Oskierski et al., 2019) and high temperature alteration of ultramafic rocks (Beinlich et al., 2014; 2018). Considering mixing of Mg from bedrock mineral sources and Rayleigh fractionation during secondary mineral precipitation, Mg isotope and chemical compositions of fluids interacting with the mine tailings at Woodsreef can be best reconciled with Mg sourced from the dissolution of serpentine, olivine and brucite but not from bedrock magnesite. Different modes of hydromagnesite, formed on the surface of the tailings and in the tunnel, respectively, are associated with distinct isotopic compositions, demonstrating the sensitivity of Mg isotopic compositions to differences in Mg sources and fluid pathways. Fluid Mg

isotopic compositions can also enable estimation of secondary mineral precipitates in cases where solid samples are not accessible (Oelkers et al., 2019; Zhang et al., 2019). Given that secondary phase formation and the effects associated with Rayleigh-type and kinetic Mg isotope fractionation can be further constrained in future studies, Mg isotopes may be used to quantify contributions from different mineral sources of Mg, thereby providing a key indicator for the efficiency of CO_2 mineralisation in ultramafic rocks.

7. Acknowledgements

H.C.O. thanks the School of Engineering and IT and the College of Science, Health, Engineering and Education, Murdoch University, for financial support via the NSSG and Small Grant schemes, respectively and acknowledges the Murdoch University Facility for Isotopes. H.C.O. also acknowledges the facilities, and the scientific and technical assistance of the Australian Microscopy & Microanalysis Research Facility at the Centre for Microscopy, Characterisation & Analysis, The University of Western Australia, a facility funded by the University, State and Commonwealth Governments. Funding for this work was provided by an Australian Research Council DECRA Fellowship and grants from Carbon Management Canada and the New South Wales Department of Industry to S.A.W., and by the French national programmes INSU-LEFE and INSU-SYSTER to V.M. Work by C.C.T. was supported by an Australian Postgraduate Award. We would like to thank Matthew Fantle, John Hooker, SR Kimmig and the anonymous reviewers for their constructive comments, which have led to significant improvement of the manuscript.

8. References

Aitchison J.C., Ireland T.R., (1995) Age profile of ophiolitic rocks across the Late Paleozoic New England Orogen, New South Wales: implications for tectonic models. Aust. J. Earth Sci. 42, 11–23.

Ashley P.M. (1997) Silica-carbonate alteration zones and gold mineralisation in the Great Serpentinite Belt, New England Orogen, New South Wales. In Tectonics and Metallogenesis of the New England Orogen (eds. P. M. Ashley and P. G. Flood). Geol. Soc. Aust. Spec. Pub. 19, 212–225.

Assima G.P., Larachi F., Molson J., Beaudoin G. (2014) Comparative study of five Quebec ultramafic mining residues for use in direct ambient carbon dioxide mineral sequestration. Chem. Eng. J. 245, 56-64.

Barnes S.J., Fiorentini M.L., Fradon M.C. (2012) Platinum group element and nickel sulphide ore tenors of the Mount Keith nickel deposit, Yilgarn Craton, Australia. Miner Deposita 47: 129-150.

Beaudoin G., Nowamooz A., Assima G.P., Lechat K., Gras A., Entezari A., Kandji E.H.B., Awoh A.-S., Horswill M., Turcotte S., Larachi F., Dupuis C., Molson J., Lemieux J.-M., Maldague X., Plante B., Bussiere B., Constantin M., Duchesne J., Therrien R., Fortier R. (2017) Passive mineral carbonation of Mg-rich mine wastes by atmospheric CO_2. Energy Proc. 114, 6083-6086.

Beaufort D., Rigault C., Billon S., Billault V., Inoue A., Inoue S., Patrier P. (2015) Chlorite and chloritisation processes through mixed-layer mineral series in low-temperature geological systems – a review. Clay Min. 50, 497-523.

Beinlich A., Austrheim H. (2012) In situ sequestration of atmospheric CO2 at low temperature and surface cracking of serpentinized peridotite in mine shafts. Chem. Geol. 332-333, 32–44.

Beinlich A., Mavromatis V., Austrheim H., Oelkers E.H. (2014) Inter-mineral Mg isotope fractionation during hydrothermal ultramafic rock alteration–Implications for the global Mg-cycle. Earth Planet. Sci. Lett. 392, 166–176.

Beinlich A., Austrheim H., Mavromatis V., Grguric B., Putnis C.V., Putnis A. (2018) Peridotite weathering is the missing ingredient of Earth's continental crust composition. Nature Comm. 9, No. 634.

Boschi C., Dini A., Baneschi I., Bedini F., Perchiazzi N., Cavallo A. (2017) Brucite-driven CO2 uptake in serpetinized dunites (Ligurain Ophiolites, Montecastelli, Tuscany). Lithos 288-289, 264-281.

Brown R.E., Brownlow J.W., Krynen J.P. (1992) Manilla–Narrabri 1:250 000 Metallogenic Map SH/56–9, SH/55–12, Metallogenic Study and Mineral Deposit Data Sheets. NSW Geol. Surv., Metallogenic Map. Ser.

Bruni J., Canepa M., Chiodini G., Cioni R., Cipolli F., Longinelli A., Marini L., Ottonello G. and Vetuschi Zuccolini M. (2002) Irreversible water–rock mass transfer accompanying the generation of the neutral, Mg-HCO3 and high pH, Ca-OH spring waters of the Genova province, Italy. Appl. Geochem. 17, 455–474.

Cawood P. A., Pisarevsky S. A. and Leitch E. C. (2011) Unravelling the New England orocline, east Gondwana accretionary margin. Tectonics 30-5, TC5002.

Cipolli F., Gambardella B., Marini L., Ottonello G., Zuccolini M.V. (2004) Geochemistry of high pH waters from serpentinites of the Gruppo di Voltri (Genova, Italy) and reaction path modelling of CO2 sequestration in serpentinite aquifers. Appl. Geochem., 19-5, 787–802.

Davis M. (2008) The CO_2 Sequestration Potential of the Ultramafic Rocks of the Great Serpentinite Belt, New South Wales. (Honours Thesis) Department of Earth Sciences, University of Newcastle.

DePaolo D.J., Kyte F.T. Marshall B.D., O'Neil J.R., Smit J. (1983) Rb-Sr, Sm-Nd, K-Ca, O, and H isotopic study of Cretaceous-Tertiary boundary sediments, Caravaca, Spain: evidence for an oceanic impact site. Earth Planet. Sci. Lett. 64-3, 356-373.

De Obeso J.C., Santiago Ramos D.P., Higgins J.A., Kelemen P.B. (2020) A Mg isotopic perspective on the mobility of magnesium during serpentinization and carbonation of the Oman ophiolite. JGR Solid Earth. https://doi.org/10.1029/2020JB020237

Eberl D., Farmer V., Barrer R. (1984) Clay mineral formation and transformations in rocks and soils. Philos. Trans. R. Soc. London Ser. A, Math. Phys. Sci. 311, 241-257.

Ebner F., Hippler D., Dietzel M., Mali H. (2019) Mg-Isotopie in Magnesiten – eine Pilotstudie fuer den Lagerstaetten-Isotopenkatalog Oesterreichs. Berg Huettenmaenn. Monatsh. 164-2, 77-83.

Glen R.A., Butt B.C. (1981) Chrysotile asbestos at Woodsreef, New South Wales. Econ. Geol. 76, 1153–1169.

Gras A., Beaudoin G., Molson J., Plante B., Bussiere B., Lemieux J.M., Dupont P.P. (2017) Isotopic evidence of passive mineral carbonation in mine wastes from the Dumont Nickel Project (Abitibi, Quebec). Int. J. Greenhouse Gas Control 60, 10-23.

Grguric B.A., Madsen I.C., Pring A. (2001) Woodalite, a new chromium analogues of iowaite from the Mount Keith nickel deposit, Western Australia, Mineral. Mag. 65-3, 427-435.

Harrison A.L., Power I.M., Dipple G.M. (2013) Accelerated carbonation of brucite in mine tailings for carbon sequestration. Environ. Sci. Technol. 47, 126-134.

Harrison A.L., Mavromatis V., Oelkers E., Benezeth P. (2018) Isotope fractionation during Mg-carbonate mineral phase transformations. Geophys. Res. Abstracts Vol. 20, EGU2018-10543.

Harrison A.L., Mavromatis V., Oelkers E.H., Benezeth P. (2019) Solubility of the hydrated Mg-carbonates nesquehonite and dypingite from 5 to 35 ºC: Implications for CO2 storage and the relative stability of Mg-carbonates. Chem. Geol. 504, 123-135.

Harrison A.L., Benezeth P., Schott J., Oelkers E.H., Mavromatis V. (2021) Magnesium and carbon isotope fractionation during hydrated Mg-carbonate mineral phase transformations. Geochim. Cosmochim. Acta 293, 507-524.

Hin R.C., Coath C.D., Carter P.J., Nimmo F., Lai Y.J., Pogge von Strandmann P.A.E., Willbold M., Leinhardt Z.M., Walter M.J., Elliott T. (2017) Magnesium isotope evidence that accretional vapour loss shapes planetary compositions. Nature 549, 511.

Huang K.J., Teng F.Z., Wei G.J., Ma J. L., Bao Z.Y. (2012) Adsorption- and desorption-controlled magnesium isotope fractionation during extreme weathering of basalt in Hainan Island, China. Earth Planet. Sci. Lett. 359, 73–83.

Huang J., Li S.-G., Xiao Y., Ke S., Li W.-Y., Tian Y. (2015) Origin of low δ^{26}Mg Cenozoic basalts from South China Block and their geodynamic implications. Geochim. Cosmochim. Acta 164, 298-317.

Immenhauser A., Buhl D., Richter D., Niedermayr A., Riechelmann D., Dietzel M., Schulte U. (2010) Magnesium-isotope fractionation during low-Mg calcite precipitation in a limestone cave—Field study and experiments. Geochim. Cosmochim. Acta 74, 4346–4364.

Jin J., Zimmerman A.R., Martin J.B., Khadka M.B. (2015) Spatiotemporal variations in carbon dynamics during a low flow period in a carbonate karst watershed: Santa Fe River, Florida, USA. Biogeochem. 122, 131-150.

Kelemen P.B., Matter J., Streit E.E., Rudge J.F., Curry W.B., Blusztajn J. (2011) Rates and mechanisms of mineral carbonation in peridotite: Natural processes and recipes for enhanced, in situ CO_2 capture and storage. Annu. Rev. Earth Planet. Sci. 39, 545-576.

Lai Y.-J., Pogge von Strandmann P.A.E., Dohmen R., Takazawa E., Elliott T. (2015) The influence of melt infiltration on the Li and Mg isotopic composition of the Horoman Peridotite Massif. Geochim. Cosmochim. Acta 164, 318-332.

Laughton C.A., Green N. (2002) The Woodsreef Magnesium Project — an example of sustainable mineral waste processing from mined ore and its utilisation to produce refined metal products. Green Processing Conference, Cairns, Qld, 29–31 May 2002.

Li W., Chakraborty S., Bear B.L., Romanek C.S., Johnson C.M. (2012) Magnesium isotope fractionation during precipitation of inorganic calcite under laboratory conditions. Earth Planet. Sci. Lett. 333-334, 304-216.

Liu P.-P., Teng F.-Z., Dick H.J.B., Zhou M.F., Chung S.-L. (2017) Magnesium isotopic composition of the oceanic mantle and oceanic Mg cycling. Geochim. Cosmochim. Acta 206, 151-165.

Maher K., Johnson N.C., Jackson A., Lammers L.N., Torchinsky A.B., Weaver K.L., Bird D.K., Brown Jr. G.E. (2016) A spatially resolved surface kinetic model for forsterite dissolution. Geochim. Cosmochim. Acta 174, 313-334.

Mavromatis V., Pearce C.R., Shirokova L.S., Bundeleva I.A., Pokrovsky O.S., Benezeth P., Oelkers, E.H. (2012) Magnesium isotope fractionation during hydrous magnesium carbonate precipitation with and without cyanobacteria. Geochim. Cosmochim. Acta 76, 161–174.

Mavromatis V., Gautier Q., Bosc O., Schott J. (2013) Kinetics of Mg partition and Mg stable isotope fractionation during its incorporation in calcite. Geochim. Cosmochim. Acta 114, 188–203.

Mavromatis V., Prokushkin A.S., Pokrovsky O.S., Viers J., Korets M.A. (2014a) Magnesium isotopes in permafrost-dominated Central Siberian larch forest watersheds. Geochim. Cosmochim. Acta 147, 76-89

Mavromatis V., Meister P., Oelkers E.H., (2014b). Using stable Mg isotopes to distinguish dolomite formation mechanisms: A case study from the Peru Margin. Chem. Geol. 385, 84–91.

Mavromatis V., Rinder T., Prokushkin A.S., Pokrovsky O.S., Korets M.A., Chmeleff J., Oelkers E.H. (2016) The effect of permafrost, vegetation, and lithology on Mg and Si isotope composition of the Yenisey River and its tributaries at the end if the spring flood, Geochim. Cosmochim. Acta 191, 32-46.

Mavromatis V., Immenhauser A., Buhl D., Purgstaller B., Baldermann A. and Dietzel M. (2017) Effect of organic ligands on Mg partitioning and Mg isotope fractionation during low temperature precipitation of calcite in the absence of growth rate effects. Geochim. Cosmochim. Acta 207, 139–153.

Mavromatis V., Power I.M., Harrison A.L., Beinlich a., Dipple G.M., Benezeth P. (2021) Mechanisms controlling the Mg isotope composition of hydromagensite-magnesite playas near Atlin, British Columbia, Canada. Chem. Geol., https://doi.org/10.1016/j.chemgeo.2021.120325

McCutcheon J., Turvey C., Wilson S.A., Hamilton J., Southam G. (2017) Experimental deployment of microbial mineral carbonation at an asbestos mine: Potential applications to carbon storage and tailings stabilization. Minerals 7 (10), 191

Mervine E.M., Wilson S.A., Power I.M., Dipple G.M., Turvey C.C., Hamilton J.L., Vanderzee S., Raudsepp M., Southam C., Matter J.M., Kelemen P.B., Stiefenhofer J., Miya Z., Southam G. (2018) Potential for offsetting diamond mine carbon emissions through mineral carbonation of processed kimberlite: an assessment of De Beers mine sites in South Africa and Canada. Min. Petrol. 112 (2), 755-765.

Milan L.A., Belousova E.A., Glen R.A., Chapman T., Kalmbach J., Fu B., Ashley P.M. (2020) A new reconstruction for Permain East Gondwana based on zircon data from ophiolite of the East Australian Great Serpentinite Belt. Geophys. Res. Lett. 48-1, e2020GL090293.

Moore O.W., Buss H.L., Green S.M., Liu M. Song Z. (2017) The importance of non-carbonate mineral weathering as a soil formation mechanism within a karst weathering profile in the SPECTRA Critical Zone Observatory, Guizhou Province, China. Acta Geochim. 36-3, 566-571.

Mumpton F.A., Thompson C.S. (1966) The Stability of Brucite in the Weathering Zone of the New Idria Serpentinite. Clays Clay Min., 14(1), 249-257.

Oelkers E.H., Berninger U.N., Perez-Fernandez A., Chmeleff J., Mavromatis V. (2018) The temporal evolution of magnesium isotope fractionation during hydromagnesite dissolution, precipitation, and at equilibrium. Geochem. Cosmochim. Acta 226, 36-49.

Oelkers E.H., Butcher R., Pogge von Strandmann P.A.E., Schuessler J.A., von Blanckenburg F., Snaebjoernsdottir S.A., Mesfin K., Aradottir E.S., Gunnarson I., Sigfusson B., Gunnlaugsson E., Matter J.M., Stute M., Gislason S.R. (2019) Using stable Mg isotopes signatures to assess the fate of magnesium during the in situ mineralization of CO_2 and H_2S at the CarbFix site in SW-Iceland. Geochim. Cosmochim. Acta 245, 542-555.

O'Hanley D.S., Offler R. (1992) Characterisation of multiple serpentinisation, Woodsreef, New South Wales. Can. Mineral. 30, 1113–1126.

O'Neil J.R., Barnes I. (1971) C_{13} and O_{18} compositions in some fresh-water carbonates associated with ultramafic rocks and serpentinites: western United States. Geochim. Cosmochim. Acta 35, 687–697.

Opfergelt S., Georg R.B., Delvausx B., Cabidoche Y.M., Burton K.W., Halliday A.N. (2012) Mechanisms of magnesium isotope fractionation in volcanic soil weathering sequences, Guadeloupe. Earth Planet. Sci. Lett. 341, 176-185.

Opfergelt S., Burton K.W., Georg R.B., West A.J., Guicharnaud R.A., Sigfusson B., Siebert C., Gislason S.R., Halliday A.N. (2014) Magnesium retention on the soil exchange complex controlling Mg isotope variations in soils, soil solutions and vegetation in volcanic soils, Iceland. Geochim. Cosmochim. Acta 125, 110–130.

Oskierski H.C., Dlugogorski B.Z., Jacobsen G. (2013a) Sequestration of atmospheric CO_2 in chrysotile mine tailings of the Woodsreef Asbestos Mine, Australia: Quantitative mineralogy, isotopic fingerprinting and carbonation rates. Chem. Geol. 358, 156-169.

Oskierski H.C., Bailey J.G., Kennedy E.M., Jacobsen G., Ashley P.M., Dlugogorski B.Z. (2013b) Formation of weathering-derived magnesite deposits in the New England Orogen, New South Wales, Australia: Implications from mineralogy, geochemistry and genesis of the Attunga Magnesite Deposit. Mineralium Deposita 48, 525-541.

Oskierski H.C., Dlugogorski B.Z., Jacobsen G. (2013c) Sequestration of atmospheric CO_2 in a weathering-derived, serpentinite-hosted magnesite deposit: ^{14}C tracing of carbon sources and age constraints for a refined genetic model. Geochim. Cosmochim. Acta 122, 226-246.

Oskierski H.C., Dlugogorski B.Z., Oliver T.K., Jacobsen G. (2016) Chemical and isotopic signatures of waters associated with the carbonation of ultramafic mine tailings, Woodsreef Asbestos Mine, Australia. Chem. Geol., 436, 11-23.

Oskierski H.C., Beinlich A., Mavromatis V., Altarawneh M., Dlugogorski B.Z. (2019) Mg isotope fractionation during continental weathering and low temperature carbonation of ultramafic rocks. Geochim. Cosmochim. Acta, 262, 60-77.

Palmer D.A., Wesolowski D.J. (1997) Potentiometric measurements of the first hydrolysis constant of magnesium (II) to 250 _C and 5 molal ionic strength (NaCl). J. Solut. Chem. 26, 217–232.

Paukert Vankeuren A.N., Matter J.M., Stute M., Kelemen P.B. (2019) Multitrace determination of apparent groundwater ages in peridotite aquifers within the Samail ophiolite, Sultanate of Oman. Earth Planet.Sci. Let. 516, 37-48.

Parkhurst D.L., Appelo C.A.J. (2013) Description of input and examples for PHREEQC version 3—A computer program for speciation, batch-reaction, one-dimensional transport, and inverse geochemical calculations: U.S. Geol. Surv. Techniques Methods 6, A43, 497 p., http://pubs.usgs.gov/tm/06/a43/.

Pearce C.R., Saldi G.D., Schott J., Oelkers E.H. (2012) Isotopic fractionation during congruent dissolution, precipitation and at equilibrium: Evidence from Mg isotopes. Geochim. Cosmochim. Acta 92, 170–183.

Pokharel R., Gerrits R., Schuessler J.A., Floor G.H., Gorbushina A.A., von Blanckenburg F. (2017) Mg isotope fractionation during uptake by a rock-inhabiting, model microcolonial fungus knufia petricola at acidic and neutral pH. Environ. Sci. Technol. 51, 9691-9699.

Pogge von Strandmann P.A.E., Burton K.W., James R.H., van Calsteren P., Gislason S.R., Sigfusson B. (2008) The influence of weathering processes on riverine magnesium isotopes in a basaltic terrain. Earth Planet. Sci. Lett. 276, 187–197.

Pogge von Strandmann P.A.E., Dohmen R., Marschall H.R., Schumacher J.C., Elliott T. (2015) Extreme Magnesium isotope fractionation at outcrop scale records the mechanism and rate at which reaction fronts advance. J. Petrol. 56, 33-58.

Pogge von Strandmann P.A.E., Olsson J., Luu T.-H., Gislason S.R., Burton K.W. (2019) Using Mg isotopes to estimate natural calcite compositions and precipitation rates during the 2010 Eyjafjallajökull eruption. Front. Earth Sci. 6-7, doi: 10.3389/feart.2019.00006.

Pokrovsky O.S., Schott J. (2000) Kinetics and mechanism of forsterite dissolution at 25º C and pH from 1 to 12. Geochim. Cosmochim. Acta 64, 3313–3325.

Pokrovsky O.S., Schott J. (2004) Experimental study of brucite dissolution and precipitation in aqueous solutions: surface speciation and chemical affinity control. Geochim. Cosmochim. Acta 68-1, 31–45.

Pokrovsky O.S., Schott J. (1999) Processes at the magnesium-bearing carbonates/solution interface. II. Kinetics and mechanism of magnesite dissolution. Geochim. Cosmochim. Acta 63-6, 881-897.

Poppe L.J., Paskevich V.J., Hathaway J.C., Blackwood D.S. (2001) A laboratory manual for X-ray powder diffraction. USGS Open-File Report 01-041.

Power I.M., Harrison A.L., Dipple G.M., Wilson S.A., Kelemen P.B., Hitch M., Southam G. (2013) Carbon mineralization: from natural analogues to engineered system. Rev. Mineral. Geochem. 77, 305–360.

Pronost J., Beaudoin G., Tremblay J., Larachi F., Duchesne J., Hébert R., Constantin M. (2011) Carbon sequestration kinetic and storage capacity of ultramafic mining waste. Environ. Sci. Technol. 45–21, 9413–9420.

Raschman P., Fedorockova A., Sucik G. (2007) Thermal activation of serpentine prior to acid leaching. Hydromet. 139, 149-153.

Samanta S., Dalai T.K., Pattanaik J.K., Rai S.K., Mazumdar A. (2015) Dissolved inorganic carbon (DIC) and its $\delta^{13}C$ in the Ganga (Hooghly) River estuary, India: Evidence of DIC generation via organic carbon degradation and carbonate dissolution. Geochim. Cosmochim. Acta 165, 226-248.

Sadekov A., Lloyd N.S., Misra S., D'Olivo J.P., McCulloch M. (2020) In situ Mg isotope measurements of biogenic carbonates using laser ablation multi-collector inductively plasma mass spectrometry: A new tool to understand biomineralisation. Rapid Commun. Mass Spectrom. 34, e8919.

Schott J., Mavromatis V., Fujii T., Pearce C.R., Oelkers E.H. (2016) The control of carbonate mineral Mg isotope composition by aqueous speciation: Theoretical and experimental modelling. Chem. Geol. 445, 120-134.

Shalev N., Farkas J., Fietzke J., Novak M., Schuessler J.A., Pogge von Strandmann P.A.E., Toerbe, P.B. (2018) Mg isotope interlaboratory comparison of reference materials from Earth-surface low-temperature environments. Geostand. Geoanal. Res. 42-2, 205-221.

Shirokova L.S., Mavromatis V., Bundeleva I., Pokrovsky O.S., Benezeth P., Pearce C.R., Gerarg E., Balor S., Oelkers E.H. (2011) Can Mg isotopes be used to trace cyanobacteria-mediated magnesium carbonate precipitation in alkaline lakes? Biogeosci. Discuss. 8, 6473-6517.

Shirokova L.S., Mavromatis V., Bundeleva I.A., Pokrovsky O.S., Benezeth P., Gerard E., Pearce C. R., Oelkers E.H. (2013) Using Mg isotopes to trace cyanobacterially mediated magnesium carbonate precipitation in alkaline lakes. Aquat. Geochem. 19, 1–24.

Siegrist M., Southam C., Bowman G., Wilson S.A., Southam G. (2017) Analysis of the potential for negative CO2 emission mine sites through bacteria-mediated carbon mineralisation: Evidence from Australia. Energy Proc. 114, 6124–6132

Stefansson A., Benezeth P., Schott J. (2013) Carbonic acid ionization and the stability of sodium bicarbonate and carbonate ion pairs to 200 _C – a potentiometric and spectrophotometric study. Geochim. Cosmochim. Acta 120, 600–611.

Stefansson A., Benezeth P. and Schott J. (2014) Potentiometric and spectrophotometric study of the stability of magnesium carbonate and bicarbonate pairs to 150C and aqueous inorganic carbon speciation and magnesite solubility. Geochim. Cosmochim. Acta 138, 21–31.

Streit E., Kelemen P., Eiler J. (2012) Coexisting serpentine and quartz from carbonate-bearing serpentinized peridotite in the Samail Ophiolite, Oman. Contrib. Mineral. Petrol. DOI 10.1007/s00410-012-0775-z

Teir S., Revitzer H., Eloneva S., Fogelholm C.-J., Zevenhoven R. (2007) Dissolution of natural serpentinite in mineral and organic acids. Int. J. Miner. Process. 83, 36-46.

Teng F.Z., Wadhwa M., Helz R.T. (2007) Investigation of magnesium isotope fractionation during basalt differentiation: Implications for a chondritic composition of the terrestrial mantle. Earth Planet. Sci. Lett. 261, 84–92.

Teng F.Z., Li, W.Y., Ke S., Marty B., Dauphas N., Huang S.C., Wu F.Y., Pourmand A. (2010) Magnesium isotopic composition of the Earth and chondrites. Geochim. Cosmochim. Acta 74, 4150–4166.

Thom G.M., Dipple G.M., Power I.M., Harrison A.L. (2013) Chrysotile dissolution rates: Implications for carbon sequestration. Appl. Geochem. 35, 244-254.

Tipper E.T., Galy A., Gaillardet J., Bickle M.J., Elderfield H., Carder E.A. (2006) The magnesium isotope budget of the modern ocean: Constraints from riverine magnesium isotope ratios. Earth Planet. Sci. Lett. 250, 241–253.

Tipper E.T., Gaillardet J., Louvat P., Capmas F., White A.F. (2010) Mg isotope constraints on soil pore–fluid chemistry: Evidence from Santa Cruz, California. Geochim. Cosmochim. Acta 74, 3883–3896.

Turvey C.C., Wilson S.A., Hamilton J.L., Southam G. (2017) Field-based accounting CO_2 sequestration in ultramafic mine wastes using portable X-ray diffraction. Am. Min., 102, 1302-1310.

Turvey C.C., Wilson S.A., Hamilton J.L., Tait A.W., McCutcheon J., Beinlich A., Fallon S.J., Dipple G.M. and Southam G. (2018) Hydrotalcites and hydrated Mg-carbonates as carbon sinks in serpentinite mineral wastes from the Woodsreef chrysotile mine, New South Wales, Australia:

controls on carbonate mineralogy and efficiency of CO_2 air capture in mine tailings. Int. J. Greenhouse Gas Control, 79, 38-60.

Turvey C.C. (2018) Formation, reaction rates and stability of hydrotalcite-group minerals: applications for mineral carbonation. PhD Thesis, Monash University, Australia.

Van Geldern R., Schulte P., Mader M., Baier A., Barth J.A.C. (2015) Spatial and temporal variations of pCO2, dissolved inorganic carbon and stable isotopes along a temperate karstic watercourse. Hydrol. Process. 29, 3423–3440.

Vickery N.M., Brown R.E., Percival I.G. (2010) Manilla 1:100000 Geological Sheet 9036 Explanatory Notes. NSW Geol. Surv., Maitland, Australia.

White A.F., Peterson M.L., Hochella, Jr, M.F. (1994) Electrochemistry and dissolution kinetics of magnetite and ilmenite. Geochem. Cosmochim. Acta 58-8, 1859-1875.

Wilson S.A., Dipple G.M., Power I.M., Thom J.M., Anderson R.G., Raudsepp M., Gabites J.E., Southam G. (2009) Carbon dioxide fixation within mine wastes of ultramafic hosted ore deposits: examples from the Clinton Creek and Cassiar chrysotile deposits, Canada. Econ. Geol. 104, 95–112.

Wilson S.A., Barker S.L., Dipple G.M., Atudorei V. (2010) Isotopic disequilibrium during uptake of atmospheric CO2 intomine process waters: implications for CO_2 sequestration. Environ. Sci. Technol. 44, 9522–9529.

Wilson S.A., Harrison A.L., Dipple G.M., Power I.M., Barker S.L.L., Mayer K.U., Fallo S.J., Raudsepp M., Southam G. (2014) Offsetting of CO2 emissions by air capture in mine tailings at the Mount Keith nickel mine, Western Australia: rates, controls and prospects for carbon neutral mining. Int. J. Greenhouse Gas Control 25, 121–140.

Wimpenny J., Gislason S.R., James R.H., Gannoun A., Pogge Von Strandmann P.A.E., Burton K.W. (2010) The behaviour of Li and Mg isotopes during primary phase dissolution and secondary mineral formation in basalt. Geochim. Cosmochim. Acta 74, 5259–5279.

Wombacher F., Eisenhauer A., Heuser A., Weyer S. (2009) Separation of Mg, Ca and Fe from geological reference materials for stable isotope ratio analyses by MC-ICP-MS and double-spike TIMS. J. Anal. At. Spectrom. 24, 627–636.

Yang W., Teng F.Z., Zhang H.F. (2009) Chondritic magnesium isotopic composition of the terrestrial mantle: A case study of peridotite xenoliths from the North China craton. Earth Planet. Sci. Lett. 288, 475–482.

Zhao M., Liu Z., Li H.C., Zeng C., Yang R., Chen B., Yan H. (2015) Response of dissolved inorganic carbon (DIC) and $\delta^{13}C_{DIC}$ to changes in climate and land cover in SW China karst catchments. Geochim. Cosmochim. Acta 165, 123-136.